

Internal wave coupling processes in Earth's atmosphere

Erdal Yiğit^{a,*}, Alexander S. Medvedev^{b,c}

^a*George Mason University, Fairfax, Virginia, USA*

^b*Max Planck Institute for Solar System Research, Göttingen, Germany*

^c*Institute of Astrophysics, Georg-August University Göttingen, Germany*

This review paper has been accepted for publication in *Advances in Space Research*.

Abstract

This paper presents a contemporary review of vertical coupling in the atmosphere and ionosphere system induced by internal waves of lower atmospheric origin. Atmospheric waves are primarily generated by meteorological processes, possess a broad range of spatial and temporal scales, and can propagate to the upper atmosphere. A brief summary of internal wave theory is given, focusing on gravity waves, solar tides, planetary Rossby and Kelvin waves. Observations of wave signatures in the upper atmosphere, their relationship with the direct propagation of waves into the upper atmosphere, dynamical and thermal impacts as well as concepts, approaches, and numerical modeling techniques are outlined. Recent progress in studies of sudden stratospheric warming and upper atmospheric variability are discussed in the context of wave-induced vertical coupling between the lower and upper atmosphere.

Keywords: Gravity waves, Vertical coupling, Thermosphere-ionosphere, Sudden stratospheric warming, Upper atmosphere variability

1. Introduction to Atmospheric Vertical Coupling

The structure and dynamics of the Earth's atmosphere are determined by a complex interplay of radiative, dynamical, thermal, chemical, and electrodynamic processes in the presence of solar and geomagnetic activity variations.

*Corresponding author

Email addresses: eyigit@gmu.edu (Erdal Yiğit), medvedev@mgs.mps.de (Alexander S. Medvedev)

The lower atmospheric processes are the primary concern of meteorology, while impacts of the Sun and geomagnetic processes on the atmosphere-ionosphere are the subject of space weather research. Thus, the whole atmosphere system is under the continuous influence of meteorological effects and space weather. A detailed understanding of the coupling mechanisms within the atmosphere-ionosphere is crucial for better interpreting atmospheric observations, understanding the Earth climate system, and developing forecast capabilities.

The atmosphere can be viewed as an ideal geophysical fluid that is pervaded by waves of various spatio-temporal scales. The term “internal” signifies the ability of waves to propagate “internally”, that is, vertically upward within the atmosphere, unlike “external” modes, in which all layers oscillate in sync when disturbances propagate horizontally. Internal waves exist because Earth’s atmosphere is overall stably stratified. Horizontal scales of internal waves vary from a few kilometers to the planetary circumference. Temporal scales cover a range from minutes to several days. Internal waves can propagate over large distances, and transfer momentum and energy from lower levels to much higher altitudes, thus providing an important coupling mechanism in the atmosphere. What are the impacts of these waves on the atmosphere-ionosphere system at various scales? The scientific community has increasingly been realizing that answering this question represents a crucial step toward better understanding the connections between meteorology and space weather.

Coupling processes from the lower atmosphere to the ionosphere have been the overarching goal of recent observational campaigns. One such campaign was the SpreadFEx that was conducted over the South American sector ([Abdu et al., 2009](#); [Takahashi et al., 2009](#)).

Nonlinear interactions of internal waves between themselves and with the undisturbed atmospheric flow create a complex dynamical system, in which long-range coupling processes can occur that link different atmospheric layers and redistribute energy and momentum between them. To investigate the origins and global consequences of such processes, the atmospheric layers cannot be investigated in isolation, but the atmosphere ought to be treated as a whole system. The importance of such investigations have been broadly recognized. In the Role Of the Sun and the Middle atmosphere/thermosphere/ionosphere In Climate (ROSMIC, [Lübken et al., 2014](#)) project within the SCOSTEP’s VarSITI (Variability of the Sun and Its Terrestrial Impact) program, the influence of the lower atmosphere on the upper atmosphere is designated as one of the focus topics ([Ward et al., 2014](#)). Specifically, ROSMIC’s “Cou-

pling by Dynamics” Working Group coordinates the efforts in investigating dynamically-induced vertical coupling processes in the atmosphere-ionosphere system.

Figure 1 illustrates the different regions in the atmosphere-ionosphere system taken from the empirical models of MSISE-90 and IRI-2012 ([Bilitza, 2014](#)). The characteristic distribution of the neutral temperature with height determines the major regions in the neutral atmosphere shown on the left: the troposphere, stratosphere, mesosphere, and thermosphere, where the latter is the hottest region of the neutral atmosphere. The ionosphere is characterized by the electron density profile and represents an ionized portion that is produced largely by solar irradiation, and coexists with the neutral upper atmosphere. The main ionospheric regions are D-, E, and F-regions, where the peak electron density is found within the F-region. The physical processes that influence the atmosphere-ionosphere system from below (“internal waves”) and above (“solar wind, magnetosphere, Sun”) are shown in black boxes as well. Internal waves are associated with the lower atmospheric weather (i.e., meteorological effects), and the effects caused by solar wind, magnetosphere, and Sun are termed broadly as space weather. Various atmosphere-ionosphere transient events, such as sudden stratospheric warming (SSW) and traveling atmospheric/ionospheric disturbances (TAD/TID) are depicted in gray at approximate altitudes where they typically occur. The turbopause (~ 105 km) marks the hypothetical boundary between the turbulently mixed homosphere and the heterosphere, where diffusive separation dominates.

A number of reviews on various aspects of coupling processes in the atmosphere-ionosphere system have been presented previously by various authors (e.g., [Kazimirovsky et al., 2003](#); [Altadill et al., 2004](#); [Lāstovička, 2006](#); [Forbes, 2007](#); [Lāstovička, 2009a,b](#)). The observations of long-term trends in the upper atmosphere have been brought to the attention of the scientific community in the works of [Lāstovička \(2012\)](#) and [Lāstovička \(2013\)](#). Here we focus on the role of internal waves in the coupling between the lower and upper atmosphere, and the resulting larger-scale effects. In particular, sudden stratospheric warmings and wave-induced atmospheric variability are discussed in the context of vertical coupling, as the two topics have recently come again to the meteorology and aeronomy communities’ attention. Our overarching goal is to provide a motivation for bridging gaps between scientists studying the lower, middle, and upper atmospheres. In this paper, we concentrate on the most recent studies, while providing references to the existing reviews for further details.

This review is structured in the following manner. Section 2 provides an overview of the physical properties of internal waves. Section 3 outlines the observations of wave structures in the middle and upper atmosphere. Section 4 presents modeling techniques for studying internal waves, and section 5 gives some details concerning atmospheric wave propagation and consequences for the upper atmosphere. Sections 6 and 7 discuss coupling processes during sudden stratospheric warmings (SSWs), and other effects related to upper atmosphere variability. In section 8, conclusions are given, and some open questions are highlighted.

2. Internal Wave Characteristics and Propagation

To a first approximation, atmospheric waves can be distinguished by their spatial scales. Earth’s atmosphere possesses a broad spectrum of waves ranging from very small- (e.g., gravity waves, GWs) to planetary-scale waves (tides, Rossby waves). Table 1 summarizes quantitatively the range of temporal scales for tides, gravity, planetary Rossby and Kelvin waves. Overall, internal wave periods vary from few minutes to tens of days. They also have different spatial scales. While small-scale GWs have typical horizontal wavelengths λ_H of several km to several hundred km, horizontal scales of solar tides and planetary waves are comparable to the circumference of Earth.

Although various internal waves can be excited by different mechanisms, in general, meteorological processes are the primary sources of these motions. They can propagate upward and grow in amplitude due to exponentially decreasing neutral mass density ρ (in order to satisfy wave action conservation). Therefore, although wave disturbances associated with small-scale GWs are relatively small at the source levels, their amplitudes can become significant at higher altitudes in the thermosphere, and are all subject to various dissipation processes. On the other hand, large-scale waves, such as planetary waves, can possess relatively larger amplitudes in the lower atmosphere, and can, therefore, dissipate at lower altitudes. This wave dissipation is the mechanism of transfer of momentum and energy from disturbances to the mean flow. Below, a brief characterization of some internal waves is presented.

2.1. Gravity Waves

These waves have a broad range of scales from small-scale acoustic-gravity waves to large-scale inertia-gravity waves. They are routinely seen in lidar, radar, airglow, and satellite measurements. Generated typically in the lower

atmosphere by meteorological processes, such as convection (*Song et al., 2003*), frontogenesis (*Gall et al., 1988*), nonlinear interactions (*Medvedev and Gavrilov, 1995*), and thunderstorms (*Curry and Murty, 1973*), they can propagate upward to the middle and upper atmosphere. These sources produce broad spatial and temporal spectra of GWs in the lower atmosphere. The spectra typically describe quadratic (with respect to disturbances) quantities: energy, wave action, or momentum fluxes ($\overline{u'w'}$, $\overline{v'w'}$) as functions of horizontal phase speeds c , or other spectral parameters. The fluxes $\overline{u'w'}$ and $\overline{v'w'}$ denote the vertical fluxes of the wave zonal and meridional momentum, respectively. The vertical structure of fluxes associated with a GW harmonic i can be written as (e.g., *Yigit et al., 2008*):

$$\mathbf{F} = \left\{ \frac{\overline{u'w'_i(z)}}{\overline{v'w'_i(z)}} \right\} = \left\{ \frac{\overline{u'w'_i(z_0)}}{\overline{v'w'_i(z_0)}} \right\} \cdot \frac{\rho(z_0)}{\rho(z)} \tau_i(z), \quad (1)$$

where z_0 denotes the source level; $\rho(z) = \rho(z_0) \exp[-(z - z_0)/H]$ is the background neutral mass density, H is the scale height, and τ_i is the transmissivity function for the i^{th} harmonic. Equation (1) implies that the wave momentum flux grows exponentially with height z above the source level z_0 . As GWs propagate upward, they interact with the atmospheric background continuously. The mean flow affects the propagation of GWs by modifying the transmissivity, which is given for one harmonic by

$$\tau_i(z) = \exp \left[- \int_{z_0}^z \sum_d \beta_d^i(z') dz' \right], \quad (2)$$

where β_d^i is the dissipation of wave harmonic i due to a given attenuation process denoted by d . The total dissipation is the sum of all attenuation processes taking place simultaneously:

$$\beta_{tot}(z) = \beta_{ion}(z) + \beta_{mol}(z) + \beta_{eddy}(z) + \beta_{non}(z) + \beta_{rad}(z), \quad (3)$$

where the height-dependent total dissipation $\beta_{tot}(z)$ is a sum of dissipations due to ion drag, molecular viscosity and thermal conduction (*Vadas and Fritts, 2005*), eddy viscosity, nonlinear diffusion (*Weinstock, 1982; Medvedev and Klaassen, 1995, 2000*), and radiative damping (*Holton, 1982*), as introduced in the work by *Yigit et al. (2008)*.

As seen from (1)–(3), upward GW propagation is affected by a competition between the nearly exponential growth of the momentum flux F , and dissipation acting upon the wave. This process facilitates a continuous transfer of

the wave momentum and energy to the mean flow. The resulting dynamical effect \mathbf{a} on the flow represents a body force per unit mass, that is, the acceleration/deceleration of the mean flow, which is given by the divergence of the momentum flux \mathbf{F} :

$$\mathbf{a}(z) = -\frac{1}{\rho} \frac{\partial \rho \mathbf{F}(z)}{\partial z}. \quad (4)$$

Thermal effects originating from GWs are described by heating/cooling rates per unit mass. The total thermal effect comprises an irreversible heating E due to transfer of mechanical energy into heat, and the differential heating/cooling Q caused by the downward transport of the sensible heat flux $\overline{w'T'}$:

$$Q(z) = -\frac{1}{\rho} \frac{\partial \rho \overline{w'T'}}{\partial z}, \quad (5)$$

T' being wave-induced temperature disturbances ([Medvedev and Klaassen, 2003](#); [Becker, 2004](#); [Yiğit and Medvedev, 2009](#)). The very same formalism for calculating dynamical and thermal effects can be applied to solar tides, planetary and Kelvin waves described below.

2.2. Solar Tides

Solar tides are particular types of gravity waves forced by periodic heating associated with the absorption of solar radiation in the atmosphere. The obvious period is 24 hours, however, due to the nonlinearity of the atmospheric dynamics, higher-order harmonics with frequencies $\omega_n = n\Omega$, $\Omega = 2\pi/24$ hours ($n = 2, 3$, etc.) are also excited. The first few tidal harmonics (diurnal, semidiurnal, and terdiurnal) are abundant in the middle atmosphere, and have noticeable amplitudes. Tidal disturbances can be represented globally with the Fourier series as a sum of harmonics

$$A_{ns} \cos(n\Omega t + s\lambda + \phi_{ns}), \quad (6)$$

where λ is the longitude, $s = 0, \pm 1, \pm 2, \dots$ is the zonal wavenumber, and A_{ns} and ϕ_{ns} are the amplitude and phase, correspondingly. Eastward and westward propagation correspond to $s < 0$ and $s > 0$, respectively. Equation (6) can be rewritten in terms of the local time $t_{LT} = t + \lambda/\Omega$ as

$$A_{ns} \cos[n\Omega t_{LT} + (s - n)\lambda + \phi_{ns}]. \quad (7)$$

The nomenclature of tides follows from (7). If $s = n$, oscillations are Sun-synchronous (that is, waves move westward following the apparent motion

of the Sun), and such modes are called “migrating tides”. Harmonics with $s \neq n$ are non-migrating tides, which can move either westward or eastward (depending on s and n). Such harmonics are excited due to inhomogeneity of solar radiation absorption and nonlinearity of atmospheric motions.

Tides have distinctive meridional structures defined by their propagation properties. Under the approximation of a linear, motionless, isothermal, and inviscid atmosphere, the horizontal structure of tides can be conveniently represented as a sum of the so-called Hough functions comprising symmetric and antisymmetric with respect to the equator modes. In the real atmosphere, the fundamental tidal structure no longer coincides with the Hough functions. In a practical sense, however, they are still sometimes used in data analyses, because only a few Hough modes can provide a good fit for the tidal component.

As with all gravity waves, only tides, whose intrinsic frequency $\hat{\omega} = \omega_n - s\bar{u}(a \cos \phi)^{-1}$ (a being the Earth radius, ϕ is the latitude, \bar{u} is the zonally averaged wind) exceeds the local Coriolis frequency $f = 2\Omega \sin \phi$, can propagate vertically and produce an effective coupling. For instance, the lower-frequency diurnal tide can propagate from tropospheric heights into the upper atmosphere mainly at low-latitudes (subject to the local winds \bar{u}), and is vertically trapped and rapidly decays above the excitation levels at higher latitudes. Tides are observed in the middle atmosphere and thermosphere, where they play a profound role in maintaining atmospheric variability. At the heights of the F region, strong *in situ* thermal tides are forced by the periodic heating due to absorption of solar UV and EUV radiation. These tides have a barotropic structure (no phase shift in vertical), and the diurnal mode dominates. More on the importance of tides in the upper atmosphere can be found in the review paper of [Forbes \(2007\)](#).

2.3. Planetary Waves

Planetary waves are often a synonym of Rossby waves, which appear in the atmosphere due to the latitudinal gradient of the Coriolis force that balances variations of the pressure gradient force. Their phase speed is always westward, however the group velocity can have either direction. Planetary waves manifest themselves as a meandering of jet streams, where the number of meanders gives the zonal wavenumber. Rossby waves are strongly dispersive: those having faster speeds are usually trapped and do not propagate vertically. They are called “barotropic” modes, unlike the slower moving “baroclinic” harmonics with zonal wave speeds of few cm s^{-1} . They are excited by the

instability of the tropospheric jet: barotropic (due to a horizontal wind shear) or baroclinic one (due to a vertical wind shear), correspondingly. The slowest planetary waves with the horizontal wavenumber 1 and/or 2, which are locked to particular locations, are called “quasi-stationary” waves, and are forced by surface inhomogeneities – topography and/or surface temperature. According to the dispersion relation for Rossby waves, which involves the background zonal wind velocity, the quasi-stationary waves have higher chances of propagating into the middle atmosphere and depositing their momentum and energy upon dissipation, mostly in the winter hemisphere. Rossby waves occur at middle- and high-latitudes, although they sometimes can shift to lower latitudes, and even cross the equator ([Medvedev et al., 1992](#)). Planetary waves play a profound role in the dynamics of the stratosphere. In particular, the wave momentum they deposit drives the pole-to-pole circulation. Another well-known transient phenomenon associated with planetary waves are sudden stratospheric warmings (see section 6). Higher in the atmosphere, the dynamical importance of Rossby waves reduces leaving it to gravity waves.

2.4. Kelvin Waves

Atmospheric Kelvin waves are large-scale waves that are the results of balancing the Coriolis force against the waveguide at the equator. These waves are trapped at low latitudes, their amplitudes decay steeply away from the equator, and their meridional velocity component vanishes, while the zonal one fluctuates. An important feature of Kelvin waves is that they are non-dispersive, that is, the phase speed of the wave crests is equal to the group velocity at all frequencies. The second peculiarity of atmospheric Kelvin waves is that their phase velocity is positive. Thus, Kelvin wave disturbances always propagate eastward retaining their shapes, which is a great help in detecting them.

Kelvin waves are excited by convection in the lower atmosphere, and can propagate vertically. As they dissipate in upper layers, the westerly momentum they deposit affects the mean circulation. Kelvin wave classification includes slow (periods of 10 to 20 days), fast (6 to 10 days), and ultra-fast (3 to 5 days). Slow waves play an important role in the lower stratosphere dynamics, e.g., in forcing the quasi-biennial oscillation, fast are noticeable in the entire stratosphere, while ultra-fast harmonics can reach the mesosphere and thermosphere heights, providing the coupling of the latter with the equatorial lower atmosphere. A good review of recent observations and effects

of Kelvin waves in the middle and upper atmosphere can be found in the introduction of the paper by [Das and Pan \(2013\)](#).

3. Observations of Internal Wave Activity in the Middle and Upper Atmosphere

3.1. General Characteristics of Observations

A variety of techniques is utilized to detect wave signatures in the atmosphere. To date, a combination of *in-situ* and remote sensing observational methods provides an unprecedented view of the local and global state and composition of the atmosphere. Thus, atmospheric temperature, pressure, wind fields, humidity, solar radiation flux, trace substances, electrical properties, and precipitation can be observed by these techniques. A variety of small- and large-scale structures can be identified in the measured fields, which exhibit systematic wave-like variations and, thus, are indicative of wave propagation. As more technologically sophisticated instruments with higher resolutions are built, the capability of capturing finer structures increases.

The key general characteristics of observations are error, accuracy, resolution, and signal-to-noise ratio. An error describes the statistical deviation of a measurement from the true value. An estimate of the precision of a measurement is the root mean square error. Signal-to-noise ratio is the ratio between the measured value and the background and instrument noise.

An *in-situ* measurement means that the sensor is directly in contact with the matter whose properties are to be measured, implying a certain level of interaction between the matter and the device that can affect measurements. In remote sensing, there is no direct contact between the instrument and the matter. Surface-based and in-situ observations provide only a very limited global coverage, while remote sensing methods do not have this shortcoming. They can be conducted via facilities on the ground, aircraft, and on satellites. Active sounding remote sensing techniques, such as radar and lidar, emit a beam with a known intensity and wavelength, and analyze the backscattered signal. Satellites that can incorporate multiple instruments on board provide the largest and most comprehensive global coverage, while their accuracy and temporal resolution may be less than those of *in-situ* ones. The first meteorological satellite TIROS (Television and InfraRed Observation Satellite) was launched in 1960, and enabled the first sounding of the terrestrial atmosphere from space. Nowadays, a large number of orbiters is operated around geospace.

3.2. Internal Wave Observations

Satellite observations can be utilized for characterization of gravity waves both in the lower and upper atmosphere. Figure 2 shows the global distribution of GW activity taken from Figure 3 of [Ern et al. \(2004\)](#). The upper panel gives the latitude-longitude distribution of the absolute values of GW horizontal momentum (in mPa), and the lower panel presents the average horizontal wavelengths at 25 km in June 1997 determined by the Cryogenic Infrared Spectrometers and Telescopes for the Atmosphere (CRISTA, [Offermann et al., 1999](#)) satellite. It is seen that large fluxes are concentrated in the winter hemisphere and at Northern Hemisphere low-latitudes. Observed GWs have larger average horizontal scales in the tropics than at middle- and high-latitudes. This instrument could capture waves with horizontal scales λ_H greater than 100 km.

Another example of satellite observations is given in Figure 3, which shows GW activity in the thermosphere at 400 km retrieved from the CHAMP (Challenging Minisatellite Payload) satellite ([Park et al., 2014](#)) launched in 2000. Latitude-longitude distributions of the daytime relative density perturbations induced by GWs are shown for equinox, June and December solstices at low solar activity. These authors have also constructed a map of GW activity in the thermosphere at high solar activity, and found that the gravity wave fields exhibit similar morphologies, but the amplitudes are a factor of two weaker.

Gravity waves produce fluctuations in the atmospheric airglow intensity ([Hickey et al., 1993](#)) that can be observed by imaging techniques ([Taylor, 1997](#)). [Mende et al. \(1998\)](#) have conducted satellite-born observations of 762 nm O₂ airglow. [Frey et al. \(2000\)](#) have measured GW-induced fluctuations of the hydroxyl OH band. More recently, [Tang et al. \(2014\)](#) observed high-frequency GW characteristics with an all-sky OH airglow imager based on the data from 2003–2009. They have found typical horizontal scales of 20–40 km, and phase speeds of 30–70 m s⁻¹. Incoherent scatter radar measurements suggest that gravity wave-like variations can be detected frequently in the upper atmosphere ([Oliver et al., 1997](#); [Djuth et al., 2004](#); [Livneh et al., 2007](#)).

Unlike with highly irregular GW fields, tidal characteristics are easier to obtain due to their periodicity and global-scale sizes. Tides can be observed both with satellite and ground-based techniques. Time and height variations of temperature and wind changes caused by tides can be measured continuously by incoherent scatter radars at single sites. Ground-based observations have provided information on the seasonal and interannual variations of the diurnal

and semidiurnal modes (e.g., [Yuan et al., 2006](#); [Fritts et al., 2010](#)). Despite some limitation in coverage, a global picture of tidal activity can be obtained from multiple sites ([Pancheva et al., 2002](#)).

Tidal variability can be inferred from satellite measurements of infrared brightness temperature ([Hagan and Forbes, 2002](#)). For a global coverage, satellite measurements of the Doppler-shift of airglow at different heights in the thermosphere have been conducted by the Wind Imaging Interferometer (WINDII) instrument on board UARS (Upper Atmosphere Research Satellite).

In the mesosphere and lower thermosphere (MLT), migrating and non-migrating solar tidal components in temperature and neutral winds have frequently been observed using SABER and TIDI instruments on board the Thermosphere-Ionosphere-Mesosphere Energetics and Dynamics (TIMED) satellite ([Killeen et al., 2006](#); [Wu et al., 2006](#)), and the two components could be separated from each other ([Oberheide et al., 2005](#); [Pancheva et al., 2013](#)). Usually, monthly mean tidal amplitudes and phases are derived from the observed temperature and zonal and meridional winds, and density residuals ([Oberheide and Forbes, 2008a,b](#)). In order to derive tidal signatures from satellite data, a 24-hour local time coverage is required. Along the orbit of the satellite, the longitude and the universal time vary simultaneously. Local time precession of the satellite was used to provide a full local time coverage and derive tidal signatures. Using density residuals derived from accelerometers on board CHAMP and Gravity Recovery and Climate Experiment (GRACE) satellites, tidal characteristics have been derived at exospheric altitudes ([Forbes et al., 2009](#)).

In the advent of the satellite technology, observations of internal waves have dramatically increased, providing an unprecedented global view of the activity of these waves.

4. Techniques of Modeling Internal Wave Processes

Although observations suggest that wave-like structures are continuously present in the upper atmosphere (e.g., [Djuth et al., 2004](#); [Livneh et al., 2007](#)), it is not always possible to determine their propagation and dissipation characteristics simultaneously and unambiguously. Theoretical, numerical, and global modeling studies allow for the analysis of various physical processes that influence the propagation of internal waves from their sources to regions where they strongly interact with atmospheric flow. Therefore, theoretical and

numerical approaches are crucial for understanding mechanisms of wave-flow interactions, and for better interpreting observations.

4.1. Theoretical Studies

Theoretical (analytical) studies of internal waves have a long history. They cover all aspects of wave dynamics – generation, propagation, and dissipation, and provide their basic understandings. Although theoretical approaches are, generally, possible for highly simplified models, their results are widely used for parameterizing subgrid processes unresolved by numerical models. A comprehensive review of these studies for gravity waves is given in the work of [Fritts and Alexander \(2003\)](#). In this section we briefly summarize them focusing on recent developments.

Understanding and quantification of wave sources in the lower atmosphere seem to be the most challenging part to date. Overall, internal waves are excited when air parcels experience vertical displacements in a stably stratified fluid. The main mechanisms of them in the real atmosphere include orography, convection, and jet/front systems. Flow over topography is the major source of atmospheric GWs with slow (with respect to the surface) horizontal phase speeds. These harmonics are especially important in the stratosphere, where they are responsible for “hot spots” of wave activity that are tied up to particular geographical locations ([Hoffmann et al., 2013](#)). These slow waves are easily filtered out by the mean wind, such that harmonics with larger phase velocities dominate in the middle atmosphere and thermosphere. Convective generation through various mechanisms, mostly in the tropics, is a source of fast and predominantly short GWs. Theoretical investigations that paved ways for parameterizing them in general circulation models are reviewed by [Kim et al. \(2003\)](#).

GWs are ubiquitous in the middle and upper atmosphere, and are not limited to low latitudes and/or particular hotspots. Tropospheric jet/front systems are identified as the main source of these waves. Although vertical displacements of air parcels in jets and fronts are obviously responsible for generation, the exact mechanism through which GWs are excited is not known, and is a subject of intense theoretical studies. The main candidates are geostrophic adjustment, Lighthill radiation, various instabilities and transient generation. Geostrophic adjustment implies a presence of GWs superimposed on a slower and more “balanced” flow. This leaves out the question of why they are present at first hand by simply stating that this is a fundamental property of the flow. Other theoretical mechanisms strive to

explain this. Lighthill radiation mechanism of GWs is based on an analogy with the generation of acoustic waves by vortical turbulent motions. In the heart of it lies the nonlinearity of flows, by means of which energy from slower vortical modes is transferred to fast divergent ones (gravity waves). The two mechanisms can probably be related if one extends the geostrophic adjustment to include nonlinearity. With that, a continuous competition occurs between the tendencies to distort the flow from a balanced state due to nonlinear advection, and to restore it by excitation of GWs. Remarkably, this approach yields results similar to the Lighthill expressions for wave sources (*Medvedev and Gavrilov, 1995*). A conceptually close, but analytically different approach is taken by proponents of the so-called mechanism of “spontaneous adjustment emission”. One more line of theoretical research is related to “unbalanced” instabilities, that is, such conditions under which balanced flows still remain stable, but the present infinitesimal GWs become explosively unstable. Transient generation mechanism is conceptually close to the unbalanced instabilities, but assumes that amplitudes of thus generated waves can be predicted within the linear theory. An excellent and insightful review of these theoretical developments has recently been given by *Plougonven and Zhang (2014)*.

4.2. Numerical Modeling Techniques

Numerical modeling allows for studying wave processes under more realistic and complex conditions. Two major techniques include (1) ray tracing, and (2) direct hydrodynamical simulations. Ray tracing is the least computationally expensive among them. It calculates paths of narrow wave packets centered around a harmonic with the given frequency and wavenumber through regions with varying propagation conditions. The information on wave phases is lost under this approach, and the entire field can be represented as a collection of a large number of wave packets and the corresponding very narrow beams (rays). This technique has its limitations. First, it is applicable only if the background varies slowly both spatially and temporally (compared to the wavelength and period of a given harmonic, correspondingly), and, thus, cannot be used for studying processes like wave break-up or nonlinear interactions. Secondly, because no information on wave phases exists, processes like diffraction and interference cannot be studied with the ray-tracing techniques. Moreover, mathematical singularities called “caustics” may arise when ray paths of different packets come close. The advantage of the ray tracing method is that trajectories are invariant in time, that is, it can be applied to studying

propagation of wave packets from their sources as well as for identification of sources by tracking their paths back in time. These approaches constitute direct and reverse ray tracing techniques, respectively. They are widely employed for interpretation of observations and linking wave signatures in the upper atmosphere to sources in the troposphere (e.g., [Evan et al., 2012](#); [Paulino et al., 2012](#); [Pramitha et al., 2014](#)). A convenience of the ray tracing technique is that the same model can be used in both modes ([Vadas and Fritts, 2009](#); [Vadas et al., 2009](#)). More on the application of the ray-tracing GW observations and implications for modeling can be found in the paper of [Ern et al. \(2013\)](#).

The method of direct wave simulation is based on numerical solution of the fundamental (primitive) equations of hydrodynamics, and, therefore, does not have many limitations of the ray tracing. It allows one to study various aspects of wave propagation in the entire atmosphere, including the upper thermosphere, where molecular diffusion and ion friction substantially alter the physics of waves. Normally, the hydrodynamic equations are linearized with respect to the larger-scale mean flow (still retaining nonlinear terms for disturbances). This formalism permits simulations of propagation, refraction, ducting, critical layer filtering and dissipation of internal waves under a variety of realistic background distributions of wind and temperature (e.g., [Liu et al., 2013](#); [Yua et al., 2009](#)). In certain cases, direct wave models can be applied to studying wave propagation from particular sources like tsunami ([Occhipinti et al., 2011](#)), or earthquakes ([Matsumura et al., 2011](#)). Increasing computing power enables a consideration of weak nonlinear interactions between harmonics ([Huang et al., 2014](#)), their break-ups ([Gavrilov and Kshevtskii, 2013](#)), and even turbulence formation ([Fritts et al., 2009](#)). The main challenge with the direct wave simulation method comes from the fact that GWs may have fast phase speeds, integration requires a long time, and model domains must have significant sizes. This problem is usually circumvented by imposing periodic lateral boundary conditions, which prevent the accounting for dispersion of wave packets. Extending domains of integration brings the direct wave models closer to another class of numerical tools, namely to general circulation models.

4.3. General Circulation Modeling

General Circulation Models or Global Climate Models (GCMs) are three-dimensional (3-D) complex mathematical models that solve the fundamental equations of motion, energy, and continuity on a sphere. The numerical

solutions of the conservation equations enable a simulation of the atmospheric dynamics, and an investigation of their interactions with the underlying physical, chemical, and radiative processes. The progress with digital computers in the second half of the 20th century have prompted the success of GCMs as research tools. The primitive equations are discretized and then solved numerically to simulate temporal evolution of atmospheric fields, such as wind, temperature, and density/pressure, under various boundary and external forcing conditions. In GCMs extending into the ionosphere, conservation equations for the plasma are solved in addition to the neutrals (e.g., [Gardner and Schunk, 2011](#); [Yigit et al., 2012a](#)).

Depending on the regions of the atmosphere covered by GCMs, they can either be global or limited-area ones. GCMs are also distinguished by the vertical layers they focus on: lower/middle atmosphere-, upper atmosphere- and “whole atmosphere” models. In general, lower/middle atmosphere models typically extend from the ground up to the mesosphere or lower thermosphere (e.g., [Manzini et al., 2006](#)); upper atmosphere models cover the thermosphere-ionosphere from the mesopause to exobase (e.g., [Gardner and Schunk, 2011](#)). Whole atmosphere models are being increasingly developed, and, as the name suggests, they perform calculations from the surface or lower atmosphere to the upper thermosphere (e.g., [Liu et al., 2010](#)). The horizontal and vertical resolutions combined with the assumed time step define the spatio-temporal capabilities of a GCM.

GCMs provide a variety of advantages. One of them is the ability to conduct control simulations. In the real atmosphere, physical processes occur simultaneously, and isolating individual processes is a challenging task. In a model, one can selectively turn on and off physical processes to determine their significance. Therefore, GCMs are useful tools for aiding the interpretation of observations. GCM output is easier to analyze because it contains all simulated fields, unlike with observations, which are always limited to certain parameters and incomplete.

However, no scientific tool comes without shortcomings. First, GCMs do not solve exactly the original partial differential equations, but their algebraic approximations on a finite number of grid points, or elements, or spectral harmonics. Therefore, it is important that numerical methods are verified to ensure stability and convergence of numerical solutions to physical ones, and the model results must be validated. Because temporal and spatial resolutions of GCMs are limited, there are always scales of motions that cannot be properly resolved, and the subgrid-scale processes have to be

accounted for, or “parameterized”. For that, any type of physics that is not self-consistently captured in GCMs should be mathematically described, ideally from first principles. Some examples of parameterizations in models are cloud microphysics, convection, eddy diffusion, and gravity waves.

Older as well as many current GCMs used relatively coarse horizontal grids, typically, a few degrees in longitude and latitude. Such resolutions are sufficient for modeling large-scale waves such as solar tides, planetary and Kelvin waves, however, they are inadequate for reproducing smaller-scale GWs. This prompted the development of GW parameterizations, among which the first were of [Lindzen \(1981\)](#) and [Matsuno \(1982\)](#). The progress in computational capabilities facilitates enhancing model resolutions, thus enabling GCMs to capture larger portions of small-scale GWs. For instance, [Tomikawa et al. \(2012\)](#) have used a GCM with a T213 spectral truncation, which correspond to a 0.5625° longitude-latitude resolution.

Overall, state-of-the-art GCMs become increasingly more sophisticated and complex in comparison with their predecessors. They include more physical processes, higher resolution to capture dynamics at smaller scales, and can be coupled together with other numerical models to form so-called “climate system models”. An example of such model, are whole atmosphere GCMs extending from the surface to the upper thermosphere (e.g., [Liu et al., 2010, 2013a](#)).

Development of GCMs requires extensive efforts typically by a group of researchers. There are community models that are available to a broader community. National Center for Atmospheric Research (NCAR) Community Climate System Model is freely available to scientists worldwide. Extensive support is provided to help guide users. This modeling framework is a product of collaboration between researchers at NCAR and their national and international collaborators. On the other hand, there are models that originate from a specific research group. For example, the Ground-to-topside Model of Atmosphere and Ionosphere for Aeronomy (GAIA) is a full atmosphere-ionosphere model that has been developed at Kyushu University.

Some applications of numerical and GCM methods in the context of the investigations of wave effects in the upper atmosphere are presented in the next section.

5. Wave Propagation and Consequences in the Upper Atmosphere

Internal waves affect the momentum, energy, and composition balance of the middle atmosphere through a variety of effects (e.g., see reviews by [Fritts and Alexander, 2003](#); [Becker, 2011](#)). Observational and modeling studies have shown that small-scale GWs (e.g., [Yigit et al., 2009](#)) and solar tides (e.g., [Oberheide et al., 2009](#)) can directly propagate to the upper atmosphere as well. We next focus on the upward propagation of these waves from the lower atmosphere to the thermosphere-ionosphere system, and the resulting effects.

5.1. Gravity Wave Effects

Earlier studies extensively employed theoretical calculations and numerical simulations to characterize GW propagation and dissipation in the thermosphere-ionosphere ([Volland, 1969](#); [Hooke, 1970](#); [Klostermeyer, 1972](#); [Hickey and Cole, 1988](#)). Recent numerical studies include more physical processes under more realistic atmospheric conditions. In particular, the response of the thermosphere-ionosphere to localized GW sources in the lower atmosphere have been investigated. [Vadas and Liu \(2009\)](#) have considered the dissipation of GWs originated from a deep convective plume in Brazil. They found that the resulting localized momentum deposition is the source of large-scale secondary GWs and traveling ionospheric disturbances. The effects of GW dissipation in the thermosphere have recently been a subject of detailed studies employing direct wave simulation models ([Hickey et al., 2009, 2010](#); [Walterscheid, 2013](#); [Heale et al., 2014](#)).

While theoretical studies and idealized numerical simulations can provide only a limited insight into gravity wave propagation and effects in the upper atmosphere, GCMs calculate four-dimensional geophysical fields that can offer a more comprehensive view of the global atmosphere and coupling mechanisms therein. However, until recently, GW propagation to the thermosphere-ionosphere has been studied with GCMs to a lesser extent. The reason for that is a combination of the following limitations: (1) Gravity waves that are capable of directly propagating from the lower atmosphere into the upper atmosphere are rather small-scale and short-period, and cannot be captured to a large extent in GCMs; (2) Middle and upper atmosphere models were detached: the former extended only up to the mesosphere (e.g., [Boville and Randel, 1992](#); [Beagley et al., 1997](#); [Manzini et al., 2006](#)), while the latter had their lower boundaries at around 80–90 km (e.g., [Roble et al., 1988](#); [Richmond et al., 1992](#)); (3) GW parameterizations have primarily been designed for

middle atmosphere models, and did not account for wave dissipation processes appropriate for the atmosphere above the turbopause (e.g., [Alexander and Dunkerton, 1999](#)). The deficiencies of the existing GW parameterizations were addressed by [Yiğit et al. \(2008\)](#), who have developed an “extended nonlinear spectral” GW scheme suitable for use in whole atmosphere models.

For the first time, [Yiğit et al. \(2009\)](#) have implemented the extended parameterization into the Coupled Middle Atmosphere and Thermosphere-2 GCM (CMAT2, [Yiğit, 2009](#)), and simulated a global view of the small-scale GW propagation into the thermosphere. Figure 4 compares the altitude-latitude cross-sections of the zonal mean zonal momentum deposition (“GW drag”, upper row), and ion drag (lower row) during a solstice. In the first “cut-off” simulation (EXP1), GW effects above the turbopause were neglected, which is similar to the use of conventional middle atmosphere parameterizations. The second simulation (EXP2) with the GW scheme turned on at all heights demonstrates that the subgrid-scale nonorographic GWs of the tropospheric origin are not only non-negligible in the thermosphere, but produce dynamical effects that are comparable to those by ion drag in the F region.

Thermal effects (heating and cooling rates) of lower atmospheric GWs in the thermosphere are also significant. Figure 5 shows the altitude-latitude cross-sections of the calculated irreversible heating rates due to dissipating GW harmonics, and the total heating/cooling rates (that include the differential heating and cooling in addition to the irreversible heating) from the work of [Yiğit and Medvedev \(2009\)](#). The former is comparable with the Joule heating (Figure 5c), and the latter with the cooling by molecular thermal conduction (Figure 5d). Note that ion drag and Joule heating are known to be two major dynamical and thermal processes in the upper atmosphere ([Killeen, 1987](#); [Wilson et al., 2006](#); [Yiğit and Ridley, 2011a](#)). Thus, global effects of GWs compete with the effects of ion-neutral coupling in the upper atmosphere, and cannot be neglected.

Further GCM studies with the implemented extended GW scheme have provided more insight into the propagation of GWs into the thermosphere during equinoctial seasons ([Yiğit et al., 2012b](#)) as well as during periods of high solar activity ([Yiğit and Medvedev, 2010](#)). Figure 6 shows their results for the mean zonal GW drag (panels a and b) and total GW heating/cooling (panels c and d) at low (left, EXP1) and high solar activity (right, EXP2). Maximum propagation altitude and thermospheric effects of lower atmospheric GWs are very sensitive to solar activity. During high solar activity, GWs propagate to altitudes of up to 450 km at high-latitudes, and produce mean

effects of up to $240 \text{ m s}^{-1} \text{ day}^{-1}$. At low solar activity, the mean effects are overall larger, in particular, in the winter hemisphere, but the penetration of GWs into the thermosphere is lower in altitude.

Higher resolution GCMs extending into the thermosphere have recently been applied to simulate GW propagation and dissipation. [Miyoshi and Fujiwara \(2008\)](#) have used a spectral surface-to-exobase GCM with a T85 ($1.4^\circ \times 1.4^\circ$ longitude-latitude) resolution to examine GW characteristics in the mesosphere and thermosphere. They found that a great portion of shorter-period (and faster) GWs penetrate from the lower atmosphere to the heights of the F layer. More recently, [Miyoshi et al. \(2014\)](#) employed the same gravity wave-resolving model to estimate the magnitudes and patterns of GW activity, momentum deposition (“wave drag”) in the thermosphere. Their results confirmed those first obtained by [Yigit et al. \(2009\)](#) and [Yigit et al. \(2012b\)](#) for the solstitial and equinoctial conditions. These results provided conclusive evidences not only of the dynamical importance of GWs propagating to the thermosphere from below, but also that their thermospheric effects can be successfully captured by parameterizations in lower-resolution GCMs. Such GWs affect the ionosphere as well. Recently, [Shume et al. \(2014\)](#)’s observational studies indicated that GWs forcing could have been responsible for short-period electrojet oscillations observed over Brazil.

Direct effects of the lower atmospheric acoustic-gravity waves on the upper atmosphere are observed distinctly during earthquakes/tsunamis as well (e.g., [Heki and Ping, 2005](#)). For example, the investigation of the Sumatra and Tohoku-Oki tsunamis have revealed detailed dynamical effects of GWs, which had not been anticipated before (e.g., [Makela et al., 2011](#); [Roland et al., 2011](#)).

5.2. Tidal Effects

Although, a significant portion of the tidal energy is absorbed in the lower thermosphere, further propagation of tidal signatures occur beyond the turbopause. Tides of lower atmospheric origin can be observed in the thermosphere by satellites ([Oberheide and Forbes, 2008b](#)), and their effects on the thermospheric composition have been derived, for example, from the data obtained with the TIMED and SNOE satellites ([Oberheide and Forbes, 2008a](#)). A number of researchers have provided evidences for tidal modulation of the low-latitude thermosphere (e.g., [Lühr et al., 2007](#); [Forbes et al., 2009](#); [Liu et al., 2009](#); [Oberheide et al., 2009](#)). [Kwak et al. \(2012\)](#) have identified the signatures of the wavenumber-three eastward travelling nonmigrating diurnal

DE3) in the thermosphere, and concluded that they are a persistent feature of the thermosphere during low solar activity.

Oberheide et al. (2009) have studied the question of how much of the tidal signatures propagates directly to the upper atmosphere. They have analyzed data from the TIMED in the MLT, and CHAMP satellite at ~ 400 km, using the Hough Mode Extension technique. Figure 7 from their work demonstrates a direct propagation of the DE3 tide from the MLT to the upper thermosphere in terms of the vertical amplitude distribution for the tidal disturbances of the field variables (T, ρ, u, v, w) . The panels a–e show that the DE3 variations of temperature extend higher into the upper thermosphere than those of other fields in (ρ, u, w) , although the density fluctuations have a secondary peak around 400 km.

Global effects of lower atmospheric tides can be readily investigated with whole atmosphere models. Their impacts can be estimated by turning on and off the tidal activity in the lower atmosphere (*Yamazaki and Richmond, 2013*). Using a GCM extending from the ground to the exobase, *Miyoshi et al. (2009)* have shown that the solar terminator wave observed by CHAMP in the thermosphere is generated mainly by the superposition of upward propagating migrating tides with wavenumbers 4–6. *Jin et al. (2011)* employed a whole atmosphere-ionosphere GCM to investigate the relationship between the wavenumber four structure and upward propagation of the nonmigrating tides. Global response of the ionosphere to the upward propagating tides from below has been investigated by *Pancheva et al. (2012)* using the GAIA GCM along with the COSMIC observations. They have determined three altitude regions of enhanced electron density in the thermosphere-ionosphere, and discovered the evidence that the wavenumber four ionospheric longitudinal structure is not solely generated by DE3 tide.

6. Vertical Coupling during Sudden Stratospheric Warmings

In this section, we focus on the observed and modeled effects of sudden stratospheric warmings (SSWs) on the upper atmosphere. SSWs are spectacular transient events in the winter Northern Hemisphere (NH) first discovered by *Scherhag (1952)*. The winter polar temperature dramatically increases within a few days following the breakdown or weakening of the stratospheric polar vortex as a consequence of planetary wave amplification and breaking. Such warmings are accompanied by deceleration, and even reversals of the westerly zonal mean zonal winds at 10 hPa (~ 30 km). *Matsuno (1971)* was

the first to demonstrate with a simple dynamical numerical model that planetary waves and their interactions with the zonal mean flow are responsible for SSWs. Further numerical studies confirmed [Matsuno \(1971\)](#)’s conclusion qualitatively ([Holton, 1976](#); [Palmer, 1981](#)). [Schoeberl \(1978\)](#) provides one of the earliest reviews of the theory and observation of stratospheric warmings focusing on the middle atmosphere.

An observation of stratospheric conditions at 10 hPa during the major SSW that took place in the winter of 2008–2009 is shown in Figure 8 adopted from the work by [Goncharenko et al. \(2010\)](#). At 10 hPa, the zonal mean temperature at the Northern winter Pole increases from 200 K to more than 260 K within a few days. This warming is accompanied by a reversal of the zonal mean winds from westerly ($> 60 \text{ m s}^{-1}$) to easterly ($< -20 \text{ m s}^{-1}$) at the same altitude, and is defined as a “major” warming. If the winter pole warms up significantly, and the zonal mean zonal jet weakens, but does not reverse, the event is said to be a “minor” warming.

Sudden changes of the morphology of the troposphere-stratosphere during SSWs ([Limpasuva et al., 2004](#)), and the accompanying effects at higher altitudes provide a natural laboratory where atmospheric vertical coupling processes can be investigated. An increasing number of global observations indicate that SSW effects can be detected beyond the stratosphere, that is, in the mesosphere-thermosphere-ionosphere. Strong upper atmosphere effects have been detected, in particular, during quiet magnetospheric conditions. Using Millstone Hill incoherent radar data on ion temperatures, warming in the lower thermosphere and cooling above 150 km were observed during a minor SSW by [Goncharenko and Zhang \(2008\)](#). [Chau et al. \(2009\)](#) observed a significant amount of semidiurnal variations in the $\mathbf{E} \times \mathbf{B}$ vertical ion drifts in the equatorial ionosphere during the winter 2007–2008 minor warming. [Goncharenko et al. \(2010\)](#) have investigated the impact of the 2008–2009 major warming on the Equatorial Ionization Anomaly (EIA). Their analysis of GPS data at low-latitudes showed that a few days before the onset of the warming, appreciable local time variations were present in the magnitude of EIA. [Pedatella and Forbes \(2010\)](#) observed significant enhancement of the nonmigrating semidiurnal westward propagating tide with the zonal wavenumber one (SW1) during the 2009 SSW. Observational evidence from satellite measurements for the dynamical coupling between the lower and upper atmosphere during SSWs have been provided by [Funke et al. \(2010\)](#). [Pancheva and Mukhtarov \(2011\)](#) have found a systematic negative response of ionospheric plasma parameters (f_0F_2 , h_mF_2 , and n_e) to an SSW, in the

COSMIC (Constellation Observing System for Meteorology Ionosphere and Climate) data.

More recently, [Goncharenko et al. \(2013\)](#) have investigated the day-to-day variability of the midlatitude ionosphere during the major SSW of 2010, and discussed the occurrences of various wave structures in the upper atmosphere during the warming. They found enhanced semidiurnal and terdiurnal variations, and raised the question of how these signals can propagate from the stratosphere to the thermosphere. [Kurihara et al. \(2010\)](#) observed significant short-term variations during a major SSW in the lower thermospheric zonal wind and temperature retrieved from the EISCAT UHF radar in high-latitudes. Motivated by the previous observational findings, modeling efforts of [Liu et al. \(2013a\)](#) demonstrated an appreciable local time and height dependence of the upper atmospheric response to SSWs. Recently, SSW effects on the upper atmosphere are being increasingly studied in the Southern Hemisphere as well (e.g., [Jonah et al., 2014](#)).

Dramatic changes in the zonal mean zonal winds \bar{u} in the stratosphere have a great impact on the propagation and dissipation of GWs, primarily due to the alteration of the GW intrinsic phase speed, $c - \bar{u}$. The evolution of large-scale wind field \bar{u} during SSWs can successfully be reproduced by GCMs (e.g., [Charlton and Polvani, 2007](#); [de la Torre et al., 2012](#), and references therein), thus, providing an opportunity for establishing a link between SSWs and variations of GW activity at altitudes up to the lower thermosphere ([Liu and Roble, 2002](#); [Yamashita et al., 2010](#)). Applying this modeling approach, [Yigit and Medvedev \(2012\)](#) investigated for the first time the global propagation of subgrid-scale GWs from the lower atmosphere to the thermosphere above the turbopause during a minor warming. Figure 9 shows the altitude-universal time distributions of the zonally averaged a) GW activity, b) GW drag, and c) large-scale zonal wind. The two white vertical lines denote the SSW period, over which these quantities experience significant changes. An enhanced propagation into the thermosphere causes an amplification of the eastward GW momentum deposition in the lower and upper thermosphere by up to a factor of 6, which, in turn, affects the zonal mean wind.

As more small-scale GW harmonics propagating from below reach the thermosphere during SSW events, they strongly impinge on the larger-scale flow upon their breaking and/or saturation. [Yigit et al. \(2014\)](#) have investigated the GW-induced small-scale variability in the high-latitude thermosphere over the life cycle of a minor SSW. Figure 10 presents the short-period (excluding tides) temporal variability of the simulated zonal wind at Northern Hemi-

sphere high-latitudes at 250 km during the different phases of the warming. The upper panel shows the results of the simulation, in which GWs were allowed to propagate all the way up into the thermosphere, and the lower panel is for the control simulation with GW propagation terminated above the turbopause. It is seen that GWs from below are responsible for a $\pm 50\%$ change in the small-scale variability of the resolved zonal wind.

7. Upper Atmosphere Variability

The term “variability” implies an existence of a mean state \bar{s} with respect to which deviations s' are studied. Since any field s is the superposition of the mean and deviations, $s = \bar{s} + s'$, the choice of the mean \bar{s} determines the spatio-temporal structure of the variability s' . The practical importance of variability is that it is a source of uncertainty in the prognosis of the atmosphere-ionosphere. The upper atmosphere is a highly variable region at all temporal and spatial scales ranging from minutes to decades, and from local to global scales. There are numerous technical challenges in studying natural variability. It is not always easy to fully capture this variability due to observational and numerical constraints. Global models always have a limited resolution. Distinguishing between a physical and non-physical variability could be an observational challenge. Because of that, and the fact that GW signatures often have no well-defined wave-like structures, the variability can be studied as an additional characteristic of the wave field.

One of the spectacular upper atmosphere features is the variability of thermospheric vertical winds. Large vertical motions are continuously present in the upper atmosphere ([Price et al., 1995](#); [Ishii et al., 2001](#)) with appreciable variations ([Innis and Conde, 2001](#)). GCM studies have indicated that nonhydrostatic effects are crucial in the spatio-temporal variability of vertical winds ([Yigit and Ridley, 2011b](#); [Yigit et al., 2012a](#)).

Overall, the variability is observed not only in neutral winds and temperature, but also in composition ([Kil et al., 2011](#)), ion flows ([Bristow, 2008](#)), electric fields ([Kozelov et al., 2008](#)), and Joule heating ([Rodger et al., 2001](#)). Besides the inherent variability due primarily to the nonlinearity of the underlying dynamics and physics, several sources external to the thermosphere-ionosphere have been identified. They are changes in (1) the solar irradiation, (2) magnetospheric forcing, and (3) the lower atmosphere. The first two are typically designated as “space weather influences” from above, while the latter is the “meteorological forcing” from below. Despite the

growing amount of observational data, separating the contributions of each mechanism to the overall variability is quite a challenging task. Concerning the subject of this review, one can state that studies of the variability due to the dynamical coupling from below are still at their infancy, although the potential of the lower atmosphere to contribute to the observed upper atmosphere variability has already been recognized (*Rishbeth, 2006*).

How can the lower atmosphere influence the upper atmosphere variability? There are a few pathways/physical mechanisms through which the lower atmospheric variability imprints on the thermosphere-ionosphere system. One of them is the direct penetration of highly irregular GWs from below. Observations have revealed a continuing presence and persistence of such waves, some of which have been discussed in this paper, but more was given in the review paper of *Fritts and Lund (2011)*. Due to the enhanced dissipation by molecular diffusion of harmonics with shorter vertical wavelengths, mostly fast harmonics with longer vertical scales can survive the propagation to the upper thermosphere. They can often manifest themselves as traveling ionospheric disturbances (TIDs) (e.g., *Fujiwara and Miyoshi, 2009*). Planetary and ultra-fast Kelvin wave signatures are also observed in the thermosphere, although their vertical extent to the upper thermosphere is strongly terminated by dissipation (*Chang et al., 2010; de Abreu et al., 2014*).

Another mechanism of small-scale variability is associated with GW breaking, which occurs at scales much smaller than the wavelength. Localized events not only permeate the flow, but also give rise to short-period and long (fast) waves. Such mechanism of secondary excitation has been extensively studied (e.g., *Vadas et al., 2003; Chun and Kim, 2008*), and found to be a likely source of harmonics that can effectively propagate into the upper thermosphere (*Vadas and Liu, 2011*). Modulation of gravity wave propagation in the middle atmosphere, e.g., during sudden stratospheric events (*Yiğit et al., 2014*), or by enhanced dissipation during periods of increased solar activity (*Yiğit and Medvedev, 2010*) can influence the upper atmosphere variability. GWs can influence the degree of ion-neutral coupling primarily by modulating ion-neutral differential velocities. Depending on the degree of GW penetration into the thermosphere and the plasma flow patterns, such modulating can constitute a significant source of variability (*Yiğit et al., 2014*).

The third pathway does not require a direct wave propagation to the upper atmosphere, but involves a chain of additional physical mechanisms to imprint lower atmospheric inhomogeneities onto the upper layers. A notable example is the wavenumber-four longitudinal structure of the low-latitude ionosphere

seen in electron density and temperature, nitric oxide density, and F-region neutral winds (see [Ren et al., 2010](#), for more observational evidences). It was suggested in the work by [Immel et al. \(2006\)](#) that the nonmigrating diurnal tide with the wavenumber-three traveling eastward is the main source of the wavenumber-four structure. The DE3 tide is generated by the latent heat release in the tropical lower atmosphere, propagates to the MLT heights, where it reaches significant amplitudes, and can be a dominant mode of the diurnal tide during certain times ([Oberheide et al., 2011](#)). [Immel et al. \(2006\)](#) suggested that the DE3 tide modulates the ionospheric dynamo at the E-region, thus affecting electric fields in the F-region along magnetic lines, and drives the ionospheric wavenumber-four structure. GCM simulations ([Hagan et al., 2007](#)) have confirmed this mechanism, while the subsequent studies investigated its various aspects ([Ren et al., 2010](#)).

8. Open Questions and Concluding Remarks

A concise review of vertical coupling in the atmosphere-ionosphere system has been presented here, focusing on the role of internal waves as the main vertical coupling mechanism. Considerable progress has been made, over the past decade, in the appreciation of the role, which these waves play in the dynamical coupling between the lower and upper atmosphere. Internal waves include planetary Rossby and Kelvin waves, tides, and gravity waves. Due to their ability to propagate vertically, internal waves represent a dynamical link between atmospheric layers.

There are many open questions that still remain in this research area, some of which are listed below. We do not intend to compile a full list of them, but name the most basic and pressing, in our view, unresolved problems.

1. What are the momentum fluxes and spectra of internal gravity waves penetrating into the thermosphere from below?
2. Can the sources of gravity waves be parameterized in terms of large-scale fields, such that the generation can be modeled by GCMs self-consistently, rather than introduced as external tuning parameters?
3. To what degree do the external energy sources (solar irradiation, geomagnetic activity) and the associated variability in the upper atmosphere affect the middle, and even lower atmosphere? What are the dynamical mechanisms?
4. What information from the lower atmosphere is needed to predict the dynamical variability above?

Although the focus of this review has been on the Earth atmosphere, internal wave coupling has wider implications, for instance, for understanding circulations of other planets, like Mars ([Medvedev et al., 2011](#)), and Venus ([Garcia et al., 2009](#)), as well.

Acknowledgements

The work was partially supported by German Science Foundation (DFG) grant ME2752/3-1. Erdal Yiğit was partially supported by NASA grant NNX13AO36G. The authors are grateful to Art Poland at George Mason University's Space Weather Laboratory for his valuable comments on the manuscript.

References

- Abdu, M. A., E. A. Kherani, I. S. Batista, E. R. de Paula, D. C. Fritts, and J. H. A. Sobral (2009), Gravity wave initiation of equatorial spread F/plasma bubble irregularities based on observational data from the SpreadFEx campaign, *Ann. Geophys.*, *27*, 2607–2622.
- Alexander, M. J., and T. J. Dunkerton (1999), A spectral parameterization of mean-flow forcing due to breaking gravity waves, *J. Atmos. Sci.*, *56*, 4167–4182.
- Altadill, D., E. M. Apostolov and J. Boska and J. Lästovička (2004), Planetary and gravity wave signatures in the F-region ionosphere with impact on radio propagation predictions and variability, *Ann. Geophys.*, *47*, 1109–1119.
- Beagley, S. R., J. de Grandpre, J. N. Koshyk, N. A. McFarlane, and T. G. Shepherd (1997), Radiative-dynamical climatology of the first generation Canadian middle atmosphere model, *Atmos. Ocean*, *35*, 293–331.
- Becker, E. (2004), Direct heating rates associated with gravity wave saturation, *J. Atmos. Sol.-Terr. Phys.*, *66*, 683–696.
- Becker, E. (2011), Dynamical control of the middle atmosphere, *Space Sci. Rev.*, *168*, 283–314, doi:10.1007/s11214-011-9841-5.
- Bilitza, D., D. Altadill, Y. Zhang, C. Mertens, V. Truhlik, et al. (2014), The International Reference Ionosphere 2012 – a model of international collaboration, *J. Space Weather Space Clim.*, *4*, A07.
- Boville, B. A., and W. J. Randel (1992), Equatorial waves in a stratospheric gcm: Effects of vertical resolution, *J. Atmos. Sci.*, *49*, 785–801.
- Bristow, W. (2008), Statistics of velocity fluctuations observed by SuperDARN under steady interplanetary magnetic field conditions, *J. Geophys. Res.*, *113*, A11202, doi:10.1029/2008JA013203.
- Chang, L. C., S. E. Palo, H. Liu, T. Fang, , and C. S. Lin (2010), Response of the thermosphere and ionosphere to an ultra fast kelvin wave, *J. Geophys. Res.*, *115*, A00G04, doi:10.1029/2010JA015453.

- Charlton, A. J., and M. L. Polvani (2007), A new look at stratospheric sudden warmings. part i: Climatology and modeling benchmarks, *J. Clim.*, *20*, doi:10.1175/JCLI3996.1.
- Chau, J. L., B. G. Fejer, and L. P. Goncharenko (2009), Quiet variability of equatorial $E \times B$ drifts during a sudden stratospheric warming event, *Geophys. Res. Lett.*, *36*, L05101, doi:10.1029/2008GL036785.
- Chun, H.-Y., and Y.-H. Kim (2008), Secondary waves generated by breaking of convective gravity waves in the mesosphere and their influence in the wave momentum flux, *J. Geophys. Res.*, *113*, D23107, doi:10.1029/2008JD009792.
- Curry, M. J., and R. C. Murty (1973), Thunderstorm-generated gravity waves, *J. Atmos. Sci.*, *31*, 1402–1408.
- Das, U., and C. J. Pan (2013), Strong kelvin wave activity observed during the westerly phase of QBO – a case study, *Ann. Geophys.*, *31*, 581–590, doi:10.5194/angeo-31-581-2013.
- de Abreu, A. J., P. R. Fagundes, M. J. A. Bolzan, M. Gende, C. Brunini, R. de Jesus, V. G. Pillat, J. R. Abalde, and W. L. C. Lima (2014), Traveling planetary wave ionospheric disturbances and their role in the generation of equatorial Spread-F and GPS phase fluctuations during the last extreme low solar activity and comparison with high solar activity, *J. Atmos. Sol.-Terr. Phys.*, *117*, 7–19.
- de la Torre, L., R. R. Garcia, D. Barriopedro, and A. Chandran (2012), Climatology and characteristics of stratospheric sudden warmings in the whole atmosphere community climate model, *J. Geophys. Res.*, *117*, doi:10.1029/2011JD016840.
- Djuth, F. T., M. P. Sulzer, S. A. Gonzales, J. D. Mathews, J. H. Elder, and R. L. Walterscheid (2004), A continuum of gravity waves in the Arecibo thermosphere?, *J. Geophys. Res.*, *31*, L16801, doi:10.1029/2003GL019376.
- Ern, M., P. Preusse, M. J. Alexander, and C. D. Warner (2004), Absolute values of gravity wave momentum flux derived from satellite data, *J. Geophys. Res.*, *109*, D20103, doi:10.1029/2004JD004752.
- Ern, M., C. Arras, A. F. K. Fröhlich, C. Jacobi, S. Kalisch, M. Krebsbach, P. Preusse, T. Schmidt, and J. Wickert (2013), Observations and ray

- tracing of gravity waves: Implications for global modeling, in *Climate and Weather of the Sun-Earth System (CAWSES)*, edited by F.-J. Lübken, Springer Atmospheric Sciences, pp. 383–408, Springer Netherlands, doi:10.1007/978-94-007-4348-9_21.
- Evan, S., M. J. Alexander, and J. Dudhia (2012), Model study of intermediate-scale tropical inertia-gravity waves and comparison to TWP-ICE campaign, *J. Atmos. Sci.*, *69*, 591–610, doi:10.1175/JAS-D-11-051.1.
- Forbes, J. M. (2007), Dynamics of the upper mesosphere and thermosphere, *J. Meteor. Soc. Japan*, *85B*, 193–213.
- Forbes, J. M., S. L. Bruinsma, X. Zhang, and J. Oberheide (2009), Surface-exosphere coupling due to thermal tides, *Geophys. Res. Lett.*, *36*, doi:10.1029/2009GL038748.
- Frey, H. U., S. B. Mende, J. F. Arens, P. R. McCullough, and G. R. Swenso (2000), Atmospheric gravity wave signatures in the infrared hydroxyl oh airglow, *Geophys. Res. Lett.*, *27*(1), 41–44.
- Fritts, D. C., and M. J. Alexander (2003), Gravity wave dynamics and effects in the middle atmosphere, *Rev. Geophys.*, *41*(1), 1003, doi:10.1029/2001RG000106.
- Fritts, D. C., and T. C. Lund (2011), Gravity wave influences in the thermosphere and ionosphere: Observations and recent modeling, in *Aeronomy of the Earth's Atmosphere and Ionosphere*, IAGA Special Sopron Book Series, pp. 109–130, Springer Netherlands, doi:10.1007/978-94-007-0326-1_8.
- Fritts, D. C., L. Wang, J. Werne, T. Lund, and K. Wan (2009), Gravity wave instability dynamics at high Reynolds numbers. part i: wave field evolution at large amplitudes and high frequencies, *J. Atmos. Sci.*, *66*, 1126–1148, doi:10.1175/2008JAS2726.1.
- Fritts, D. C., D. Janches, H. Iimura, W. K. Hocking, N. J. Mitchell, R. G. Stockwell, B. Fuller, B. Vandepeer, J. Hormaechea, C. Brunini, and H. Levato (2010), Southern Argentina agile meteor radar: System design and initial measurements of large-scale winds and tides, *J. Geophys. Res.*, *115*, doi:10.1029/2010JD013850.

- Fujiwara, H., and Y. Miyoshi (2009), Global distribution of the thermospheric disturbances produced by effects from the upper and lower regions: simulations by a whole atmosphere gcm, *Earth Planets Space*, *61*, 463–470.
- Funke, B., M. Lopez-Puertas, D. Bermejo-Pantalen, M. Garca-Comas, G. P. Stiller, T. von Clarmann, M. Kiefer, and A. Linden (2010), Evidence for dynamical coupling from the lower atmosphere to the thermosphere during a major stratospheric warming, *Geophys. Res. Lett.*, *37*(13), doi:10.1029/2010GL043619.
- Gall, R. L., R. T. Williams, and T. L. Clark (1988), Gravity waves generated during frontogenesis, *J. Atmos. Sci.*, *45*, 2204–2019.
- Gardner, L. C., and R. W. Schunk (2011), Large-scale gravity wave characteristics simulated with a high-resolution global thermosphere-ionosphere model, *J. Geophys. Res.*, *116*, A06303, doi:10.1029/2010JA015629.
- Garcia, R. F., P. Drossart, G. Piccioni, M. Lopez-Valverde, and G. Occhipinti (2009), Gravity waves in the upper atmosphere of Venus revealed by CO₂ nonlocal thermodynamic equilibrium emissions, *J. Geophys. Res.*, *114*, doi:10.1029/2008JE003073.
- Gavrilov, N. M., and S. P. Kshevtskii (2013), Numerical modeling of propagation of breaking nonlinear acoustic-gravity waves from the lower to the upper atmosphere, *Adv. Space Res.*, *51*, 1168–1174, doi:10.1016/j.asr.2012.10.023.
- Goncharenko, L., and S.-R. Zhang (2008), Ionospheric signatures of sudden stratospheric warming: Ion temperature at middle latitude, *Geophys. Res. Lett.*, *35*, L21103, doi:10.1029/2008GL035684.
- Goncharenko, L. P., A. J. Coster, J. L. Chau, and C. E. Valladares (2010), Impact of sudden stratospheric warmings on equatorial ionization anomaly, *J. Geophys. Res.*, *115*, A00G07, doi:10.1029/2010JA015400.
- Goncharenko, L. P., V. W. Hsu, C. G. M. Brum, S.-R. Zhang, and J. T. Fentzke (2013), Wave signatures in the midlatitude ionosphere during a sudden stratospheric warming of january 2010, *J. Geophys. Res. Space Physics*, *118*, doi:10.1029/2012JA018251.

- Hagan, M. E., and J. M. Forbes (2002), Migrating and nonmigrating diurnal tides in the middle and upper atmosphere excited by tropospheric latent heat release, *J. Geophys. Res.*, *107*(D24), 4754, doi:10.1029/2001JD001236.
- Hagan, M. E., A. Maute, R. G. Roble, A. D. Richmond, T. J. Immel, and S. L. England (2007), Connections between deep tropical clouds and the earth’s ionosphere, *Geophys. Res. Lett.*, *34*, L20109, doi:10.1029/2007GL030142.
- Heale, C. J., J. B. Snively, M. P. Hickey, and C. J. Ali (2014), Thermospheric dissipation of upward propagating gravity wave packets, *J. Geophys. Res. Space Physics*, *119*, 3857–3872, doi:10.1002/2013JA019387.
- Heki, K., and J. Ping (2005), Directivity and apparent velocity of the coseismic ionospheric disturbances observed with a dense GPS array, *Earth Planet. Sci. Lett.*, *236*, 845–855.
- Hickey, M. P., and K. D. Cole (1988), A numerical model for gravity wave dissipation in the thermosphere, *J. Atmos. Terr. Phys.*, *50*, 689–697.
- Hickey, M. P., G. Schubert, and R. L. Walterscheid (1993), Gravity wave-driven fluctuations in the O₂ atmospheric (0-1) nightglow from an extended, dissipative emission region, *J. Geophys. Res.*, *98*, 13,717–13,729.
- Hickey, M. P., G. Schubert, and R. L. Walterscheid (2009), Propagation of tsunami-driven gravity waves into the thermosphere and ionosphere, *J. Geophys. Res.*, doi:10.1029/2009JA014105.
- Hickey, M. P., R. L. Walterscheid, and G. Schubert (2010), Wave mean flow interactions in the thermosphere induced by a major tsunami, *J. Geophys. Res. Space Physics*, *115*(A9), doi:10.1029/2009JA014927.
- Hoffmann, L., X. Xue, and M. J. Alexander (2013), A global view of stratospheric gravity wave hotspots located with atmospheric infrared sounder observations, *J. Geophys. Res.*, *118*, doi:10.1029/2012JD018658,.
- Hoffmann, P., C. Jacobi, and C. Borries (2012), Possible planetary wave coupling between the stratosphere and ionosphere by gravity wave modulation, *J. Atmos. Sol.-Terr. Phys.*, *75–76*, 71–80.
- Holton, J. R. (1976), A semi-spectral numerical model for wave-mean flow interactions in the stratosphere: Application to sudden stratospheric warmings, *J. Atmos. Sci.*, *33*, 1639–1649.

- Holton, J. R. (1982), The role of gravity wave induced drag and diffusion in the momentum budget of the mesosphere, *J. Atmos. Sci.*, *39*, 791–799.
- Hooke, W. H. (1970), The ionospheric response to internal gravity waves: f_2 region response, *J. Geophys. Res.*, *75*(28), 5535–5544.
- Huang, C. Y., Y.-J. Su, E. K. Sutton, D. R. Weimer, and R. L. Davidson (2014), Energy coupling during the august 2011 magnetic storm, *J. Geophys. Res. Space Physics*, *119*, doi:10.1002/2013JA019297.
- Immel, T. J., E. Sagawa, S. L. England, S. B. Henderson, M. E. Hagan, S. B. Mende, H. U. Frey, C. M. Swenson, and L. J. Paxton (2006), Control of equatorial ionospheric morphology by atmospheric tides, *Geophys. Res. Lett.*, *33*, L15108, doi:10.1029/2006GL026161.
- Innis, J. L., and M. Conde (2001), Thermospheric vertical wind activity maps derived from Dynamics Explorer-2 WATS observations, *Geophys. Res. Lett.*, *28*, 3847–3850.
- Ishii, M., M. Conde, R. W. Smith, M. Krynicki, E. Sagawa, and S. Watari (2001), Vertical wind observations with two Fabry-Perot interferometers at Poker Flat, Alaska, *J. Geophys. Res.*, *106*, 10,537–10,551.
- Jonah, O. F., E. R. de Paula, E. A. Kherani, S. L. G. Dutra, and R. R. Paes (2014), Atmospheric and ionospheric response to sudden stratospheric warming of January 2013, *J. Geophys. Res. Space Physics*, *119*, 4973–4980, doi:10.1002/2013JA019491.
- Jin, H., Y. Miyoshi, H. Fujiwara, H. Shinagawa, K. Terada, N. Terada, M. Ishii, Y. Otsuka, and A. Saito (2011), Vertical connection from the tropospheric activities to the ionospheric longitudinal structure simulated by a new earth’s whole atmosphere-ionosphere coupled model, *J. Geophys. Res. Space Physics*, *116*, doi:10.1029/2010JA015925.
- Kazimirovsky, E., M. Herraiz, and B. A. D. L. Morena (2003), Effects on the ionosphere due to phenomena occurring below it, *Surv. Geophys.*, *24*, 139–184.
- Kil, H., Y.-S. Kwak, L. J. Paxton, R. R. Meier, and Y. Zhang (2011), O and N₂ disturbances in the F region during the 20 November 2003 storm seen from TIMED/GUVI, *J. Geophys. Res.*, *116*, A02314, doi:10.1029/2010JA016227.

- Killeen, T. L. (1987), Energetics and dynamics of the earth's thermosphere, *Rev. Geophys.*, *25*, 433–454.
- Killeen, T. L., Q. Wu, S. C. Solomon, D. A. Ortland, W. R. Skinner, R. J. Niciejewski, and D. A. Gell (2006), Timed Doppler interferometer: Overview and recent results, *J. Geophys. Res. Space Physics*, *111*, doi:10.1029/2005JA011484.
- Kim, Y.-J., S. E. Eckermann, and H.-Y. Chun (2003), An overview of the past, present and future of gravity-wave drag parametrization for numerical climate and weather prediction models, *Atmos. Ocean*, *41*, 65–98.
- Klostermeyer, J. (1972), Influence of viscosity, thermal conduction, and ion drag on the propagation of atmospheric gravity waves in the thermosphere, *Z. Geophysik*, *38*, 881–890.
- Kozelov, B. V., I. V. Golovchanskaya, A. A. Ostapenko, and Y. V. Fedorenko (2008), Wavelet analysis of high-latitude electric and magnetic fluctuations observed by the Dynamic Explorer 2 satellite, *J. Geophys. Res.*, *113*, A03308, doi:10.1029/2007JA012575.
- Kurihara, J., Y. Ogawa, S. Oyama, S. Nozawa, M. Tsutsumi, C. M. Hall, Y. Tomikawa, and R. Fujii (2010), Links between a stratospheric sudden warming and thermal structures and dynamics in the high-latitude mesosphere, lower thermosphere, and ionosphere, *Geophys. Res. Lett.*, *37*, L13806, doi:10.1029/2010GL043643.
- Kwak, Y.-S., H. Kil, W. K. Lee, S.-J. Oh, and Z. Ren (2012), Nonmigrating tidal characteristics in thermospheric neutral mass density, *J. Geophys. Res. Space Physics*, *117*, doi:10.1029/2011JA016932.
- Limpasuva, V., D. W. J. Thompson, and D. L. Hartmann (2004), The life cycle of the northern hemisphere sudden stratospheric warmings, *J. Clim.*, *17*, 2584–2596.
- Lindzen, R. S. (1981), Turbulence and stress owing to gravity waves and tidal breakdown, *J. Geophys. Res.*, *86*, 9707–9714.
- Liu, H., M. Yamamoto, and H. Lühr (2009), Wave-4 pattern of the equatorial mass density anomaly: A thermospheric signature of tropical deep convection, *Geophys. Res. Lett.*, *36*, doi:10.1029/2009GL039865.

- Liu, H., H. Jin, Y. Miyoshi, H. Fujiwara, and H. Shinagawa (2013), Upper atmosphere response to stratosphere sudden warming: Local time and height dependence simulated by GAIA model, *Geophys. Res. Lett.*, *40*, doi:doi:10.1002/grl.50146.
- Liu, H.-L., and R. G. Roble (2002), A study of a self-generated stratospheric sudden warming and its mesospheric-lower thermospheric impacts using the coupled TIME-GCM/CCM3, *J. Geophys. Res.*, *107*, 15–1,15–18.
- Liu, H.-L., B. T. Foster, M. E. Hagan, J. M. McInerney, A. Maute, L. Qian, A. D. Richmond, R. G. Roble, S. C. Solomon, R. R. Garcia, D. Kinnison, D. R. Marsh, A. K. Smith, J. Richter, F. Sassi, and J. Oberheide (2010), Thermosphere extension of the Whole Atmosphere Community Climate Model, *J. Geophys. Res.*, *115*, A12302, doi:10.1029/2010JA015586.
- Liu, X., J. Xu, J. Yue, and S. L. Vadas (2013), Numerical modeling study of the momentum deposition of small amplitude gravity waves in the thermosphere, *Ann. Geophys.*, *31*, 1–14, doi:10.5194/angeo-31-1-2013.
- Livneh, D. J., I. Seker, F. T. Djuth, and J. D. Mathews (2007), Continuous quasiperiodic thermospheric waves over Arecibo, *J. Geophys. Res.*, *112*, A07313, doi:10.1029/2006JA012225.
- Lübken, F.-J., A. Seppälä, and W. E. Ward (2014), Project ROSMIC, *VarSITI Newsletter*, *1*, 7–9.
- Lühr, H., K. Häusler, and C. Stolle (2007), Longitudinal variation of f region electron density and thermospheric zonal wind caused by atmospheric tides, *Geophys. Res. Lett.*, *34*, doi:10.1029/2007GL030639.
- Lästovička, J. (2006), Forcing of the ionosphere by waves from below, *J. Atmos. Sol.-Terr. Phys.*, *68*, 479–497.
- Lästovička, J. (2009a), Lower ionosphere response to external forcing: A brief review, *Adv. Space Res.*, *43*, 1–14.
- Lästovička, J. (2009b), Global pattern of trends in the upper atmosphere and ionosphere: Recent progress, *J. Atmos. Sol.-Terr. Phys.*, *71*, 1514–1528.
- Lästovička, J. (2012), On the role of ozone in long-term trends in the upper atmosphere-ionosphere system, *Ann. Geophys.*, *30*, 811–816, doi:10.5194/angeo-30-811-2012, 2012.

- Lăstovička, J. (2013), Trends in the upper atmosphere and ionosphere: Recent progress, *J. Geophys. Res. Space Physics*, *118*, doi:10.1002/jgra.50341.
- Makela, J. J., et al. (2011), Imaging and modeling the ionospheric airglow response over Hawaii to the tsunami generated by the Tohoku earthquake of 11 March 2011, *Geophys. Res. Lett.*, *38*, L00G02, doi:10.1029/2011GL047860.
- Manzini, E., M. A. Giorgetta, M. Esch, L. Kornblueh, and E. Roeckner (2006), The influence of sea surface temperatures on the northern winter stratosphere: Ensemble simulations with the MAECHAM5 model, *J. Clim.*, *19*, 3863–3881.
- Matsumura, M., A. Saito, T. Iyemori, H. Shinagawa, T. Tsugawa, Y. Otsuka, M. Nishioka, and C. H. Chen (2011), Numerical simulations of atmospheric waves excited by the 2011 off the Pacific coast of Tohoku earthquake, *Earth Planets Space*, *63*, 885–889, doi:10.5047/eps.2011.07.015.
- Matsuno, T. (1971), A dynamical model of the stratospheric sudden warming, *J. Atmos. Sci.*, *28*, 1479–1494.
- Matsuno, T. (1982), A quasi one-dimensional model of the middle atmosphere circulation interacting with internal gravity waves, *J. Meteor. Soc. Japan*, *60*, 215–226.
- Medvedev, A. S., and N. M. Gavrilov (1995), The nonlinear mechanism of gravity wave generation by meteorological motions in the atmosphere, *J. Atmos. Terr. Phys.*, *57*, 1,221–1,231.
- Medvedev, A. S., and G. P. Klaassen (1995), Vertical evolution of gravity wave spectra and the parameterization of associated wave drag, *J. Geophys. Res.*, *100*, 25,841–25,853.
- Medvedev, A. S., and G. P. Klaassen (2000), Parameterization of gravity wave momentum deposition based on nonlinear wave interactions: Basic formulation and sensitivity tests, *J. Atmos. Sol.-Terr. Phys.*, *62*, 1015–1033.
- Medvedev, A. S., and G. P. Klaassen (2003), Thermal effects of saturating gravity waves in the atmosphere, *J. Geophys. Res.*, *108*, 4040, doi:10.1029/2002JD002504.

- Medvedev, A. S., and E. Yiğit (2012), Thermal effects of internal gravity waves in the Martian thermosphere, *Geophys. Res. Lett.*, *39*, L05201, doi:10.1029/2012GL050852.
- Medvedev, A. S., A. I. Pogoreltsev, and S. A. Suhanova (1992), Modelling the global structure of stationary planetary waves and their penetration across the equator, *Atmos. Oceanic Phys.*, *27*, 574–581.
- Medvedev, A. S., E. Yiğit, P. Hartogh, and E. Becker (2011), Influence of gravity waves on the Martian atmosphere: general circulation modeling, *J. Geophys. Res.*, *116*, E10004, doi:10.1029/2011JE003848.
- Mende, S. B., H. Frey, S. P. Geller, and G. R. Swenson (1998), Gravity wave modulated airglow observations from spacecraft, *Geophys. Res. Lett.*, *25*, 757–760.
- Miyoshi, Y., and H. Fujiwara (2008), Gravity waves in the thermosphere simulated by a general circulation model, *J. Geophys. Res.*, *113*, D011101, doi:10.1029/2007JD008874.
- Miyoshi, Y., H. Fujiwara, J. M. Forbes, and S. L. Bruinsma (2009), Solar terminator wave and its relation to the atmospheric tide, *J. Geophys. Res. Space Physics*, *114*, doi:10.1029/2009JA014110.
- Miyoshi, Y., H. Fujiwara, H. Jin, and H. Shinagawa (2014), A global view of gravity waves in the thermosphere simulated by a general circulation model, *J. Geophys. Res. Space Physics*, *119*, 5807–5820, doi:10.1002/2014JA019848.
- Oberheide, J., and J. M. Forbes (2008a), Thermospheric nitric oxide variability induced by nonmigrating tides, *Geophys. Res. Lett.*, *35*, L16814, doi:10.1029/2008GL034825.
- Oberheide, J., and J. M. Forbes (2008b), Tidal propagation of deep tropical cloud signatures into the thermosphere from timed observations, *Geophys. Res. Lett.*, *35*, L04816, doi:10.1029/2007GL032397.
- Oberheide, J., Q. Wu, D. Ortland, T. Killeen, M. Hagan, R. Roble, R. Niciejewski, and W. Skinner (2005), Non-migrating diurnal tides as measured by the TIMED Doppler interferometer: Preliminary results, *Adv. Space Res.*, *35*(11), 1911–1917.

- Oberheide, J., J. M. Forbes, K. Häusler, Q. Wu, and S. L. Bruinsma (2009), Tropospheric tides from 80 to 400 km: Propagation, interannual variability, and solar cycle effects, *J. Geophys. Res.*, *114*, D00I05, doi:10.1029/2009JD012388.
- Oberheide, J., J. M. Forbes, X. Zhang, and S. L. Bruinsma (2011), Climatology of upward propagating diurnal and semidiurnal tides in the thermosphere, *J. Geophys. Res.*, *116*, A11306, doi:10.1029/2011JA016784.
- Occhipinti, G., P. Coisson, J. J. Makela, S. Allgeyer, A. Kherani, H. Hebert, and P. Lognonne (2011), Three-dimensional numerical modeling of tsunami-related internal gravity waves in the Hawaiian atmosphere, *Earth Planets Space*, *63*, 847–851, doi:10.5047/eps.2011.06.051.
- Offermann, D., K. U. Grossmann, P. Barthol, P. Knieling, M. Riese, and R. Trant (1999), Cryogenic infrared spectrometers and telescopes for the atmosphere (CRISTA) experiment and middle atmosphere variability, *J. Geophys. Res.*, *104*, 16,311–16,325.
- Oliver, W. L., Y. Otsuka, M. Sato, T. Takami, and S. Fukao (1997), A climatology of f region gravity wave propagation over the middle and upper atmosphere radar, *J. Geophys. Res.*, *102*, 14,499–14,512.
- Palmer, T. N. (1981), Diagnostic study of a wavenumber-2 stratospheric sudden warming in a transformed Eulerian-mean formalism, *J. Atmos. Sci.*, *38*, 844–855.
- Pancheva, D., and P. Mukhtarov (2011), Stratospheric warmings: The atmosphere-ionosphere coupling paradigm, *J. Atmos. Sol.-Terr. Phys.*, *73*, 1697–1702.
- Pancheva, et al., (2002), Global-scale tidal variability during the PSMOS campaign of June–August 1999: interaction with planetary waves, *J. Atmos. Sol.-Terr. Phys.*, *64*, 1865 – 1896.
- Pancheva, D., Y. Miyoshi, P. Mukhtarov, H. Jin, H. Shinagawa, and H. Fujiwara (2012), Global response of the ionosphere to atmospheric tides forced from below: Comparison between cosmic measurements and simulations by atmosphere-ionosphere coupled model GAIA, *J. Geophys. Res. Space Physics*, *117*, doi:10.1029/2011JA017452.

- Pancheva, D., P. Mukhtarov, and A. K. Smith (2013), Climatology of the migrating terdiurnal tide (TW3) in SABER/TIMED temperatures, *J. Geophys. Res.*, *118*(4), 1755–1767, doi:10.1002/jgra.50207.
- Park, J., H. Lühr, C. Lee, Y. H. Kim, G. Jee, and J.-H. Kim (2014), A climatology of medium-scale gravity wave activity in the midlatitude/low-latitude daytime upper thermosphere as observed by CHAMP, *J. Geophys. Res. Space Physics*, *119*, doi:10.1002/2013JA019705.
- Paulino, I., H. Takahashi, S. L. Vadas, C. M. Wrasse, J. H. A. Sobral, A. F. Medeiros, R. A. Buriti, and D. Gobbi (2012), Forward ray-tracing for medium-scale gravity waves observed during the COPEX campaign, *J. Atmos. Sol.-Terr. Phys.*, *90–91*, 117–123, doi:10.1016/j.jastp.2012.08.006.
- Pedatella, N. M., and J. M. Forbes (2010), Evidence for stratosphere sudden warming-ionosphere coupling due to vertically propagating tides, *Geophys. Res. Lett.*, *37*, L11104, doi:10.1029/2010GL043560.
- Plougonven, R., and F. Zhang (2014), Internal gravity waves from atmospheric jets and fronts, *Rev. Geophys.*, *52*, 33–76, doi:10.1002/2012RG000419.
- Pramitha, M., M. V. Ratnam, A. Taori, B. V. K. Murthy, D. Pallamraju, and S. V. B. Rao (2014), Identification of gravity wave sources using reverse ray tracing over Indian region, *Atmos. Chem. Phys. Discuss.*, *14*, 19,587–19,623, doi:10.5194/acpd-14-19587-2014.
- Price, G. D., R. W. Smith, and G. Hernandez (1995), Simultaneous measurements of large vertical winds in the upper and lower thermosphere, *J. Atmos. Terr. Phys.*, *57*, 631–643.
- Ren, Z., W. Wan, J. Xiong, and L. Liu (2010), Simulated wave number 4 structure in equatorial f-region vertical plasma drifts, *J. Geophys. Res.*, *115*, A05301, doi:10.1029/2009JA014746.
- Richmond, A. D., E. C. Ridley, and R. G. Roble (1992), A thermosphere/ionosphere general circulation model with coupled electrodynamics, *Geophys. Res. Lett.*, *19*, 601–604.
- Rishbeth, H. (2006), F-region links with the lower atmosphere?, *J. Atmos. Sol.-Terr. Phys.*, *68*, 469–478.

- Roble, R. G., E. C. Ridley, and A. D. Richmond (1988), A coupled thermosphere/ionosphere general circulation model, *Geophys. Res. Lett.*, *15*(12), 1325–1328.
- Rodger, A. S., G. D. Wells, R. J. Moffett, and G. J. Bailey (2001), The variability of joule heating, and its effects on the ionosphere and thermosphere, *Ann. Geophys.*, *19*, 773781.
- Rolland, L. M., P. Lognonne, E. Astafyeva, E. Kherani N. Kobayashi, M. Mann, and H. Munekane (2011), The resonant response of the ionosphere imaged after the 2011 off the Pacific coast of Tohoku Earthquake, *Earth Planet Space*, *63*, 853–857.
- Scherhag, R. (1952), Die explosionsartige Stratosphärenenerwärmung des Spätwinters 1951-1952, *Ber. Deut. Wetterdienstes*, *6*, 51–63.
- Schoeberl, M. R. (1978), Stratospheric warmings: observation and theory, *Rev. Geophys.*, *16*, 521–538.
- Shume, E. B., F. S. Rodrigues, A. J. Mannucci, and E. R. de Paula (2014), Modulation of equatorial electrojet irregularities by atmospheric gravity waves, *J. Geophys. Res. Space Physics*, *119*, doi:10.1002/2013JA019300.
- Song, I.-S., H.-Y. Chun, and T. P. Lane (2003), Generation mechanisms of convectively forced internal gravity waves and their propagation to the stratosphere, *J. Atmos. Sci.*, *60*, 1960–1980.
- Takahashi, H., M. J. Taylor, P.-D. Pautet, A. F. Medeiros, D. Gobbi, C. M. Wrasse, J. Fechine, M. A. Abdu, I. S. Batista, E. Paula, J. H. A. Sobral, D. Arruda, S. L. Vadas, F. S. Sabbas, and D. C. Fritts (2009), Simultaneous observation of ionospheric plasma bubbles and mesospheric gravity waves during the SpreadFEx Campaign, *Ann. Geophys.*, *27*, 1477–1487.
- Tang, Y., X. Dou, T. Li, T. Nakamura, X. Xue, C. Huang, A. Manson, C. Meek, D. Thorsen, and S. Avery (2014), Gravity wave characteristics in the mesopause region revealed from oh airglow imager observations over northern Colorado, *J. Geophys. Res. Space Physics*, *119*, doi:10.1002/2013JA018955.

- Taylor, M. J. (1997), A review of advances in imaging techniques for measuring short period gravity waves in the mesosphere and lower thermosphere, *Adv. Space Res.*, *19*, 667–676.
- Tomikawa, Y., K. Sato, S. Watanabe, Y. Kawatani, K. Miyazaki, and M. Takahashi (2012), Growth of planetary waves and the formation of an elevated stratopause after a major stratospheric sudden warming in a T213L256 GCM, *J. Geophys. Res.*, *117*, D16101, doi:10.1029/2011JD017243.
- Vadas, S., and H. Liu (2009), Generation of large-scale gravity waves and neutral winds in the thermosphere from the dissipation of convectively generated gravity waves, *J. Geophys. Res.*, *114*, A10310, doi:10.1029/2009JA014108.
- Vadas, S. L., and D. C. Fritts (2005), Thermospheric responses to gravity waves: Influences of increasing viscosity and thermal diffusivity, *J. Geophys. Res.*, *110*, D15103, doi:10.1029/2004JD005574.
- Vadas, S. L., and D. C. Fritts (2009), Reconstruction of the gravity wave field from convective plumes via ray tracing, *Ann. Geophys.*, *27*, 147–177.
- Vadas, S. L., and H.-L. Liu (2011), Neutral winds and densities at the bottomside of the f layer from primary and secondary gravity waves from deep convection, in *Aeronomy of the Earth's Atmosphere and Ionosphere*, edited by M. Abdu and D. Pancheva, IAGA Special Sopron Book Series 2, pp. 131–139, Springer.
- Vadas, S. L., D. C. Fritts, and M. J. Alexander (2003), Mechanism for the generation of secondary waves in wave breaking regions, *J. Atmos. Sci.*, *60*, 194–214.
- Vadas, S. L., M. J. Taylor, P.-D. Pautet, P. A. Stamus, D. C. Fritts, H.-L. Liu, F. T. S. Sabbas, V. T. Rampinelli, P. Batista, and H. Takahashi (2009), Convection: the likely source of the medium-scale gravity waves observed in the oh airglow layer near Brasilia, Brazil, during the SPREADFEX campaign, *Ann. Geophys.*, *27*, 231–259.
- Volland, H. (1969), Full wave calculations of gravity wave propagation through the thermosphere, *J. Geophys. Res.*, *74*, 1786–1795.

- Walterscheid, R. L. (2013), The propagation of transient wave packets in highly dissipative media, *Journal of Geophysical Research: Space Physics*, *118*, 878–884, doi:10.1002/jgra.50097.
- Ward, W., F.-J. Lübken, and A. Seppälä (2014), ROSMIC, a new project in the SCOSTEP VarSITI program, in *40th COSPAR Scientific Assembly, Moscow, Russia*.
- Weinstock, J. (1982), Nonlinear theory of gravity waves: Momentum deposition, generalized Rayleigh friction, and diffusion, *J. Atmos. Sci.*, *39*, 1,698–1,710.
- Wilson, G. R., D. R. Weimer, J. O. Wise, and F. A. Marcos (2006), Response of the thermosphere to Joule heating and particle precipitation, *J. Geophys. Res.*, A10314, doi:10.1029/2005JA011274.
- Wu, Q., T. L. Killeen, D. A. Ortland, S. C. Solomon, R. D. Gablehouse, R. M. Johnson, W. R. Skinner, R. J. Niecejewski, and S. J. Franke (2006), Timed Doppler interferometer (TIDI) observations of migrating diurnal and semidiurnal tides, *J. Atmos. Sol.-Terr. Phys.*, *68*, 408–417.
- Yamashita, C., H. Liu, and X. Chu (2010), Responses of mesosphere and lower thermosphere temperatures to gravity wave forcing during stratospheric sudden warming, *Geophys. Res. Lett.*, *37*, L09803, doi:10.1029/2009GL042351.
- Yamazaki, Y., and A. D. Richmond (2013), A theory of ionospheric response to upward-propagating tides: Electrodynamical effects and tidal mixing effects, *J. Geophys. Res. Space Physics*, *118*, 5891–5905, doi:10.1002/jgra.50487.
- Yiğit, E. (2009), Modelling atmospheric vertical coupling: Role of gravity wave dissipation in the upper atmosphere, Ph.D. thesis, University College London Doctoral Thesis.
- Yiğit, E., and A. S. Medvedev (2009), Heating and cooling of the thermosphere by internal gravity waves, *Geophys. Res. Lett.*, *36*, L14807, doi:10.1029/2009GL038507.
- Yiğit, E., and A. S. Medvedev (2010), Internal gravity waves in the thermosphere during low and high solar activity: Simulation study., *J. Geophys. Res.*, *115*, A00G02, doi:10.1029/2009JA015106.

- Yiğit, E., and A. S. Medvedev (2012), Gravity waves in the thermosphere during a sudden stratospheric warming, *Geophys. Res. Lett.*, *39*, L21101, doi:10.1029/2012GL053812.
- Yiğit, E., and A. J. Ridley (2011a), Effects of high-latitude thermosphere heating at various scale sizes simulated by a nonhydrostatic global thermosphere-ionosphere model, *J. Atmos. Sol.-Terr. Phys.*, *73*, 592–600, doi:10.1016/j.jastp.2010.12.003.
- Yiğit, E., and A. J. Ridley (2011b), Role of variability in determining the vertical wind speeds and structure, *J. Geophys. Res.*, *116*, A12305, doi:10.1029/2011JA016714.
- Yiğit, E., A. D. Aylward, and A. S. Medvedev (2008), Parameterization of the effects of vertically propagating gravity waves for thermosphere general circulation models: Sensitivity study, *J. Geophys. Res.*, *113*, D19106, doi:10.1029/2008JD010135.
- Yiğit, E., A. S. Medvedev, A. D. Aylward, P. Hartogh, and M. J. Harris (2009), Modeling the effects of gravity wave momentum deposition on the general circulation above the turbopause, *J. Geophys. Res.*, *114*, D07101, doi:10.1029/2008JD011132.
- Yiğit, E., A. J. Ridley, and M. B. Moldwin (2012a), Importance of capturing heliospheric variability for studies of thermospheric vertical winds, *J. Geophys. Res.*, *117*, A07306, doi:10.1029/2012JA017596.
- Yiğit, E., A. S. Medvedev, A. D. Aylward, A. J. Ridley, M. J. Harris, M. B. Moldwin, and P. Hartogh (2012b), Dynamical effects of internal gravity waves in the equinoctial thermosphere, *J. Atmos. Sol.-Terr. Phys.*, *90–91*, 104–116, doi:10.1016/j.jastp.2011.11.014.
- Yiğit, E., A. S. Medvedev, S. L. England, and T. J. Immel (2014), Simulated variability of the high-latitude thermosphere induced by small-scale gravity waves during a sudden stratospheric warming, *J. Geophys. Res.*, *119*, doi:10.1002/2013JA019283.
- Yua, Y., M. P. Hickey, and Y. Li (2009), A numerical model characterizing internal gravity wave propagation into the upper atmosphere, *Adv. Space Res.*, *44*, 836–846, doi:10.1016/j.asr.2009.05.014.

Yuan, T., C. Y. She, M. E. Hagan, B. P. Williams, T. Li, K. Arnold, T. D. Kawahara, P. E. Acott, J. D. Vance, D. Krueger, and R. G. Roble (2006), Seasonal variation of diurnal perturbations in mesopause region temperature, zonal, and meridional winds above Fort Collins, Colorado (40.6°N, 105°W), *J. Geophys. Res. Atmos.*, *111*, doi:10.1029/2004JD005486.

Table 1: Typical temporal scales of internal waves in the terrestrial atmosphere.	
Internal wave	Typical range of temporal scales
Gravity wave	few minutes to several hours ($2\pi/f$, $f = 2\Omega \sin \phi$)
Solar tide	1, 1/2, 1/3 days
Planetary wave	2 to few tens of days
Kelvin wave	3 to 20 days

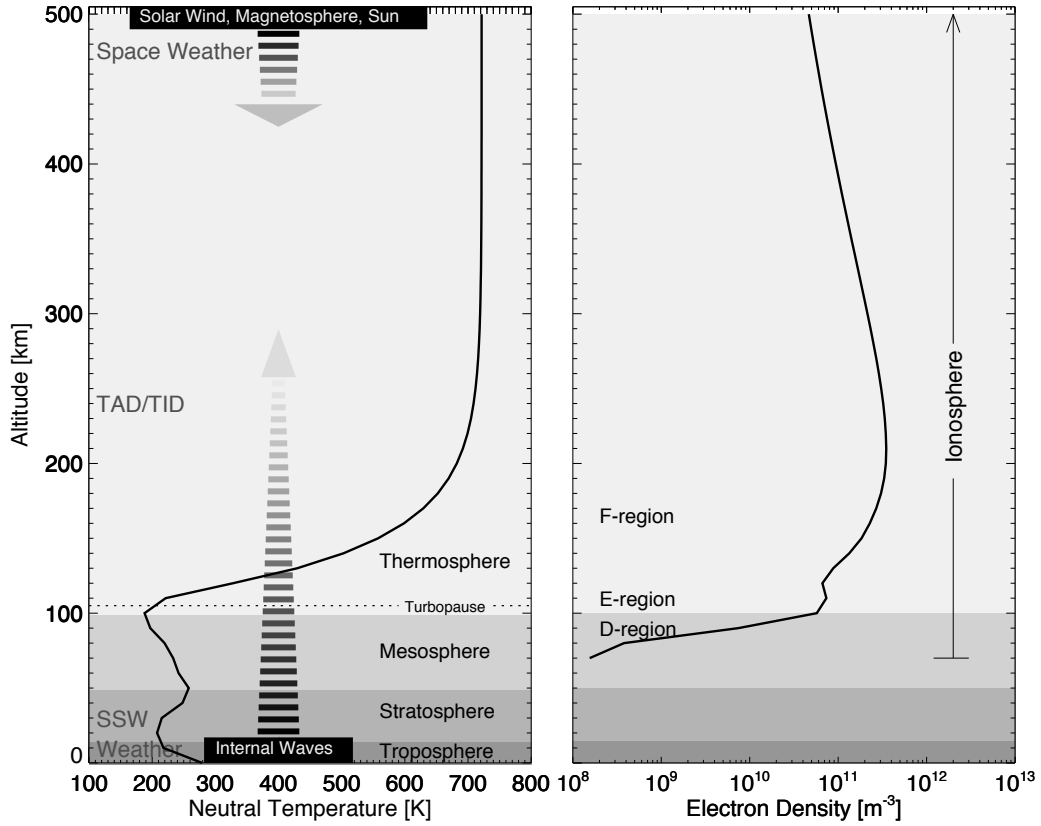


Figure 1: Vertical structure of the atmosphere-ionosphere system, where the neutral atmospheric temperature is shown on the left and the electron density distribution on the right. Panels are produced using midlatitude data from MSISE-90 and IRI 2012 models for 1 January 2010 at noon with daily $F_{10.7} = 77.2 \times 10^{-22} \text{ W m}^{-2} \text{ Hz}^{-1}$ and $A_p = 0.5$. SSW and TAD/TID denotes sudden stratospheric warming and traveling atmospheric/ionospheric disturbances, respectively. The turbopause is at about 105 km.

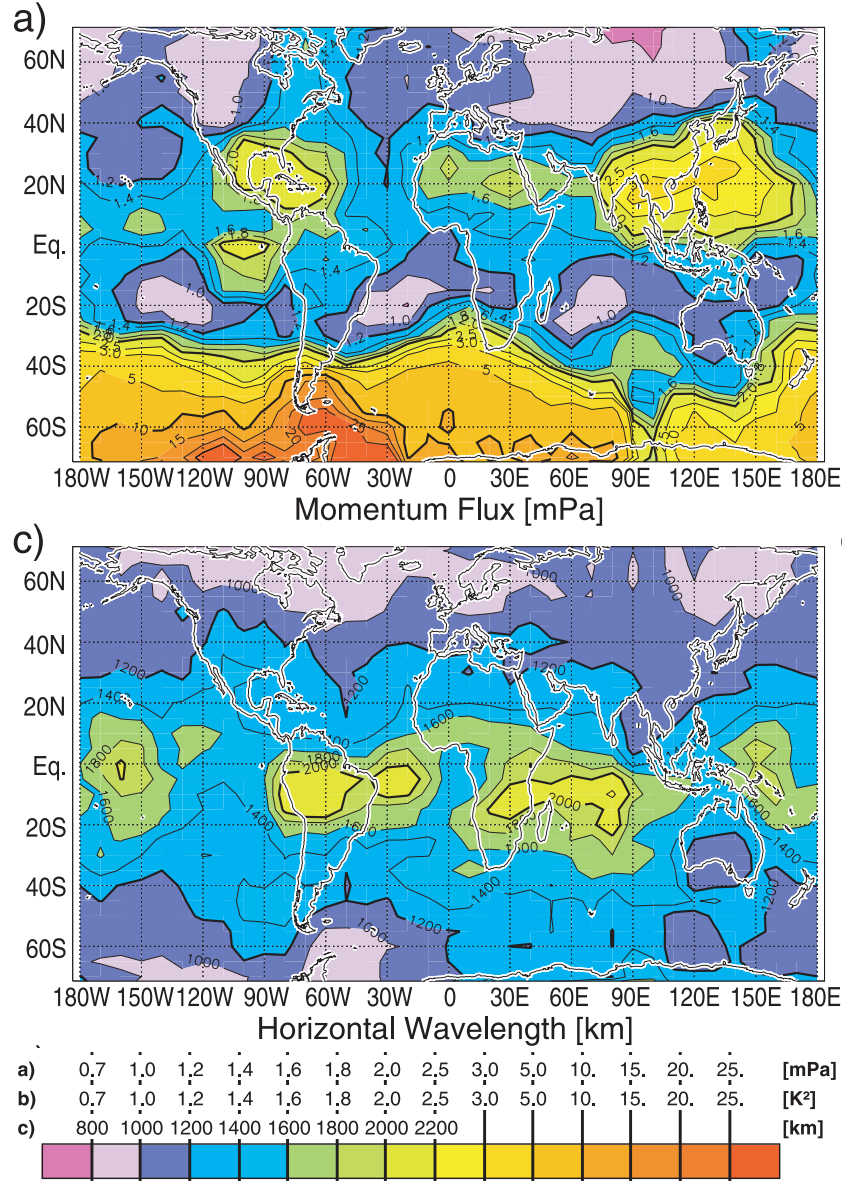


Figure 2: Absolute values of the vertical flux of horizontal gravity wave momentum in mPa (above) and average horizontal wavelengths (below) in km observed by CRISTA-2 (Cryogenic Infrared Spectrometers and Telescopes for the Atmosphere-2) at 25 km in August 1997. Adopted from Figure 3 of [Ern et al. \(2004\)](#).

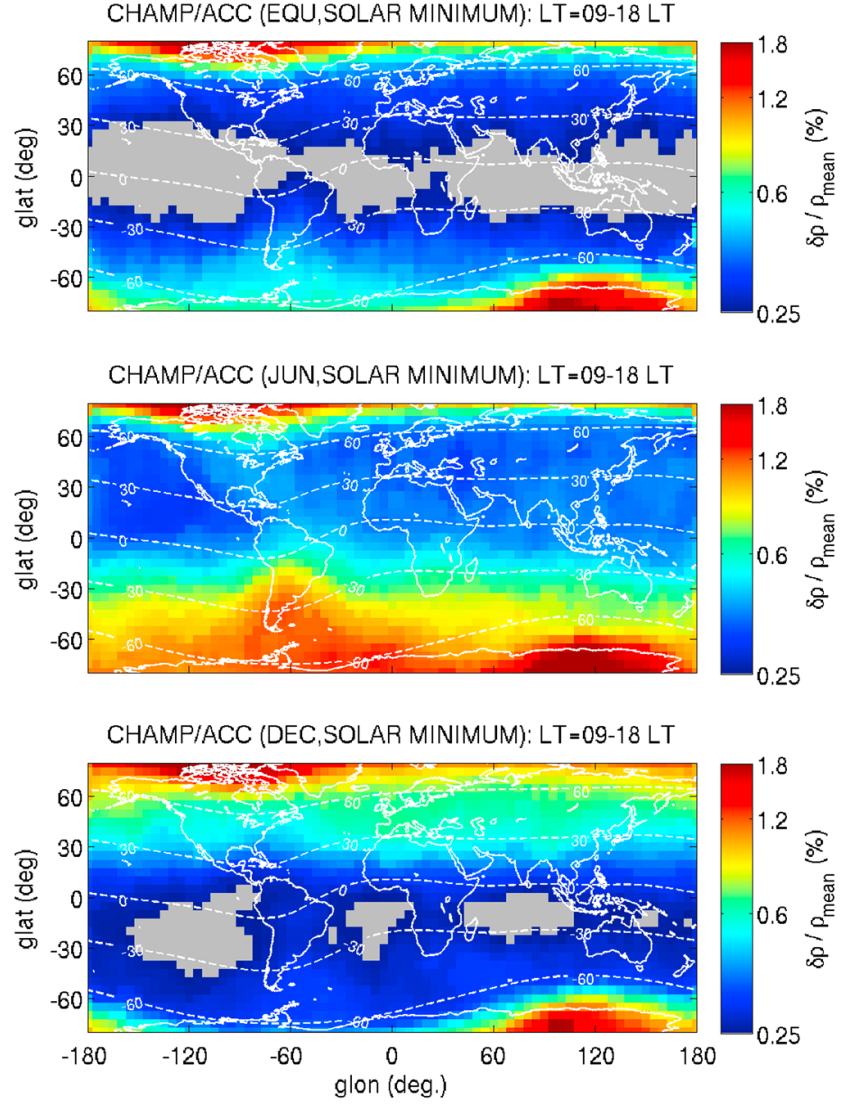


Figure 3: Day-time gravity wave activity in terms of relative density perturbations during equinox, June and December solstices based on solar minimum years (2006–2010) obtained from the CHAMP satellite (Figure 2, [Park et al., 2014](#)).

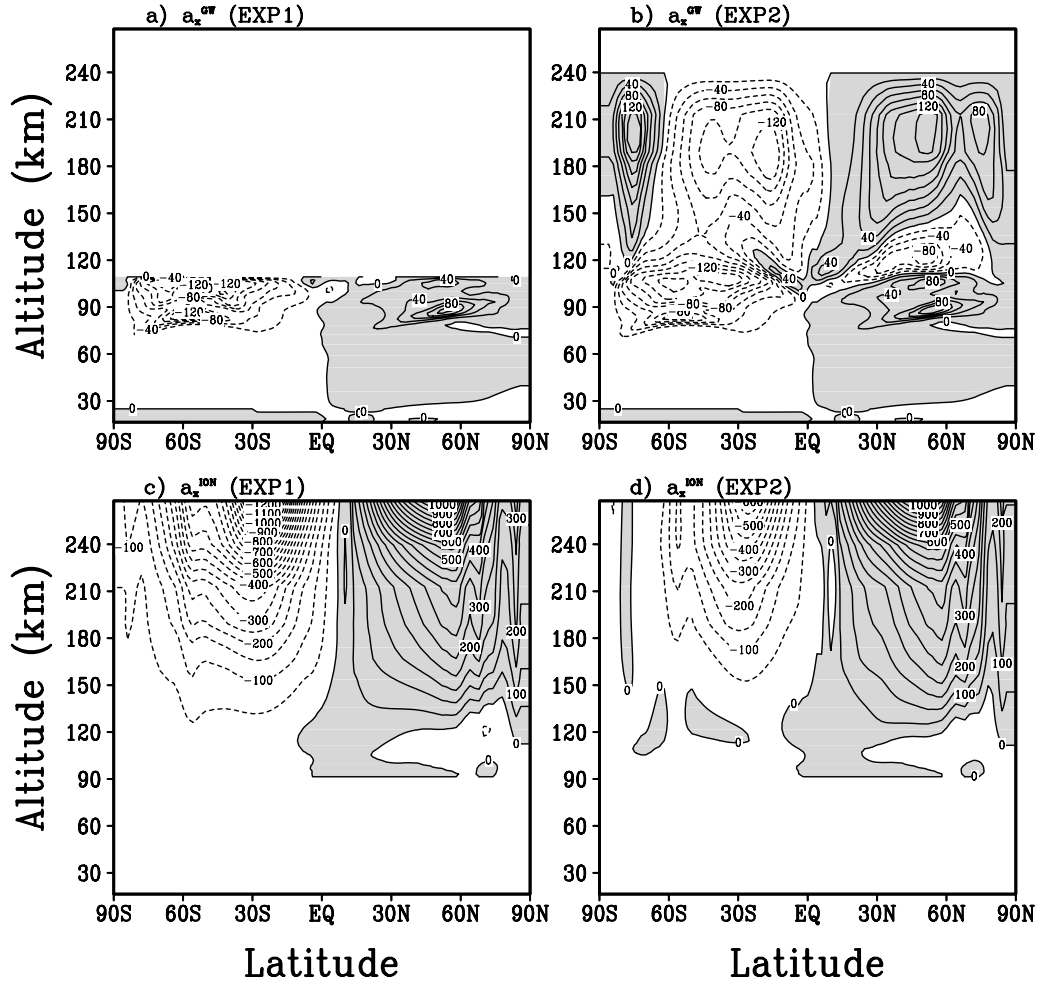


Figure 4: Altitude-latitude cross sections of the zonal mean zonal GW drag (upper panels) and ion drag (lower panels) in $\text{m s}^{-1} \text{ day}^{-1}$ in the cut-off (EXP1, left) and extended simulations (EXP2, right) with the CMAT2 GCM (Figure 3, [Yigit et al., 2009](#)).

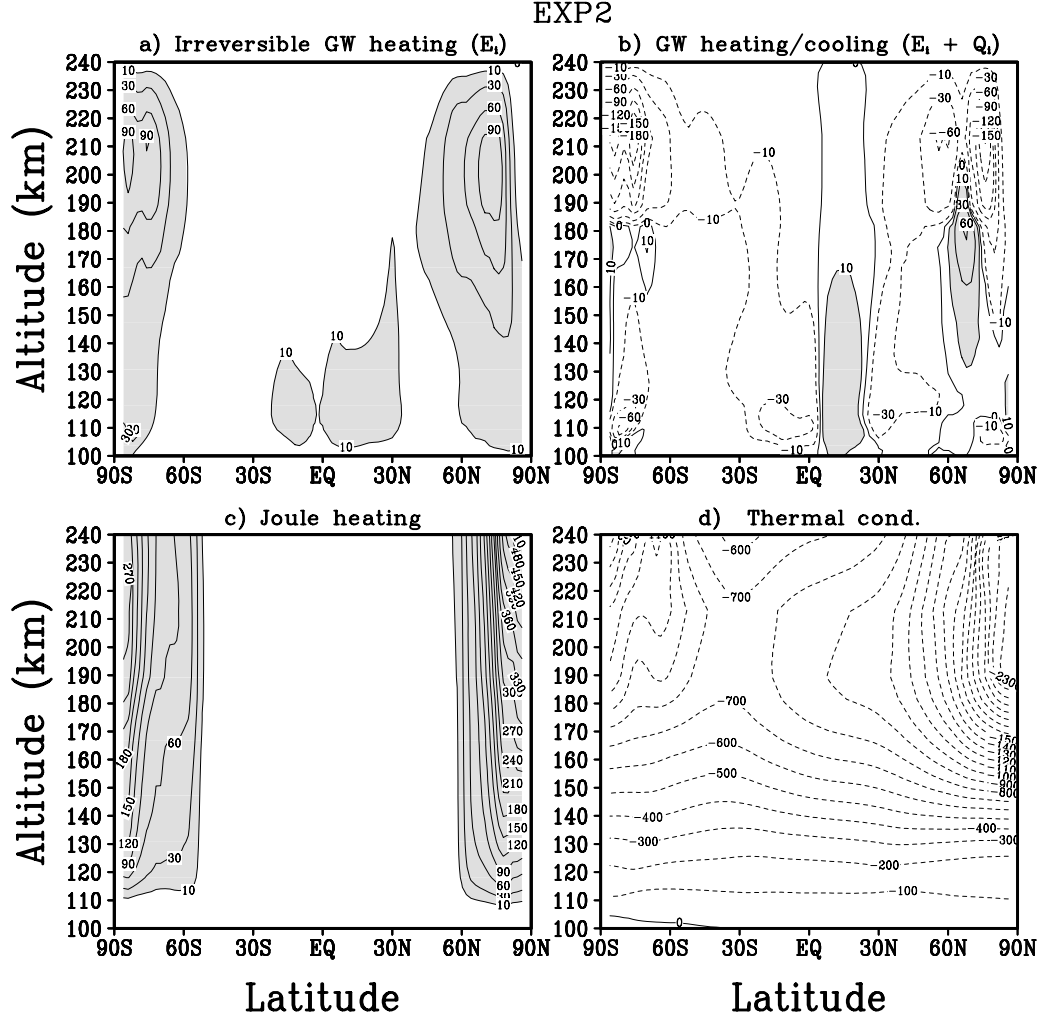


Figure 5: Altitude-latitude cross sections of the mean zonal mean a) GW irreversible heating, b) GW heating/cooling, c) ionospheric Joule heating, and d) cooling by thermal conduction in K day^{-1} for June solstice at low solar activity simulated by the CMAT2 GCM, implementing the extended nonlinear gravity scheme (Figure 2, [Yiğit and Medvedev, 2009](#)).

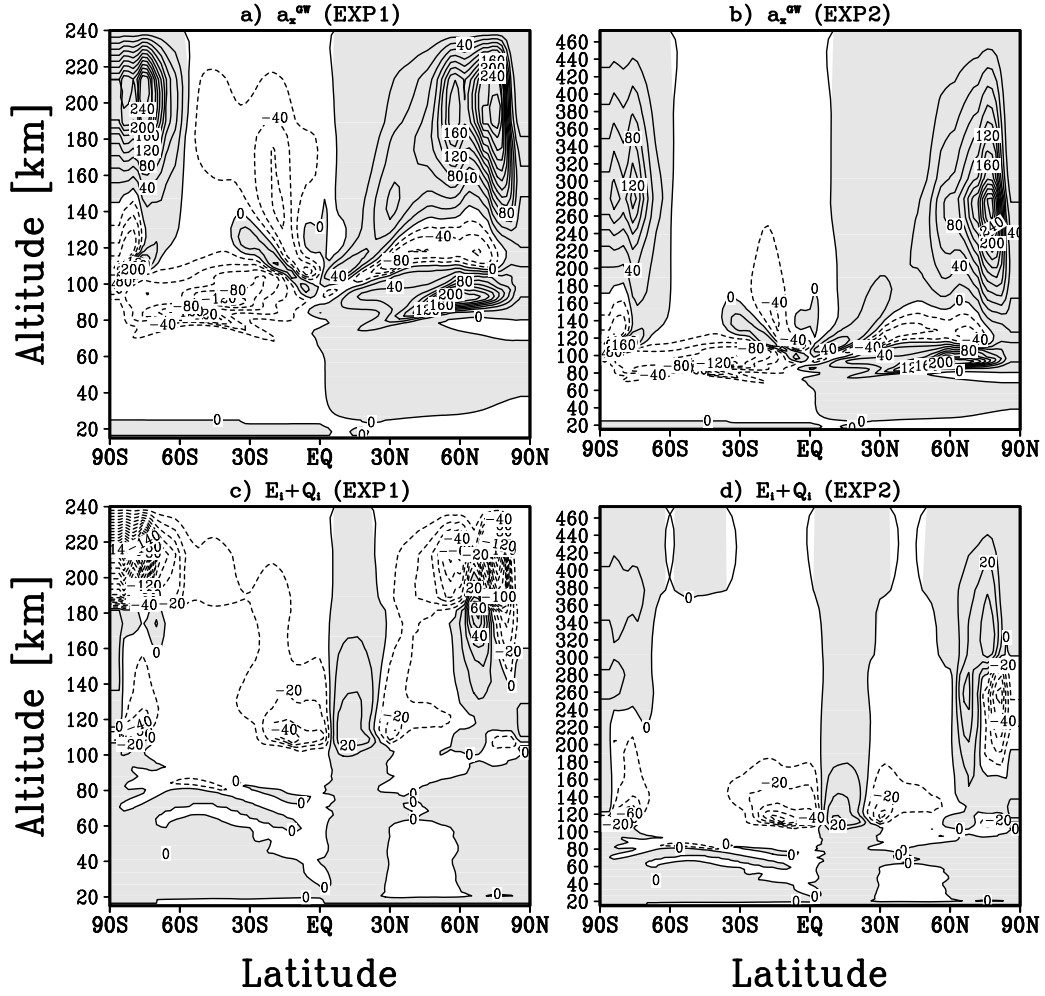


Figure 6: Altitude-latitude cross-sections of the mean zonal mean GW drag (panels a and b) and total GW heating/cooling (panels c and d) at low (left, EXP1) and high solar activity (right, EXP2) simulated with CMAT2 using the extended nonlinear scheme (Figure 10, [Yigit and Medvedev, 2010](#)).

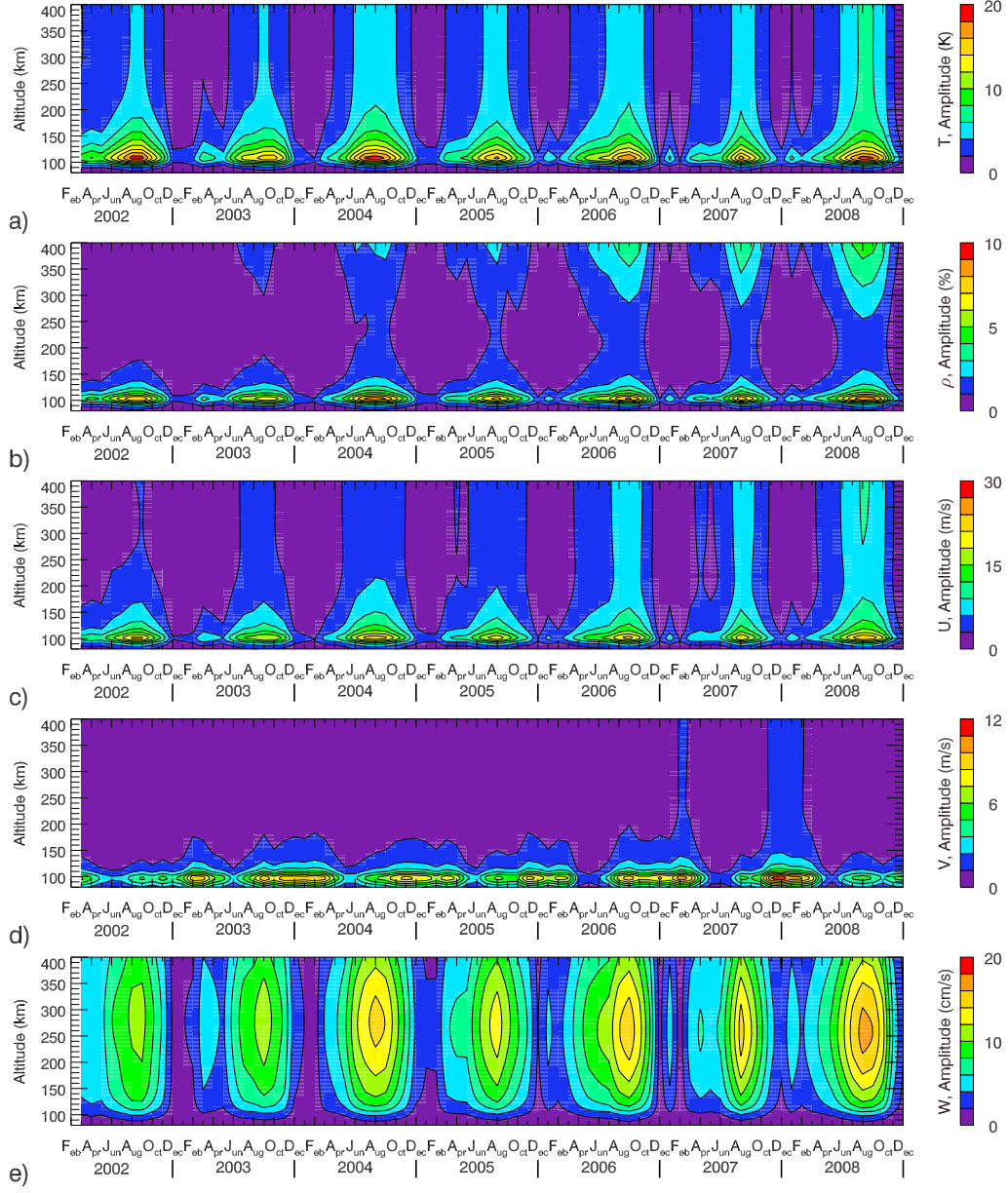


Figure 7: DE3 tidal propagation into the thermosphere in terms of the tidal amplitudes for the temperature, density, zonal wind, meridional wind, and vertical wind (Figure 13, [Oberheide et al., 2009](#)).

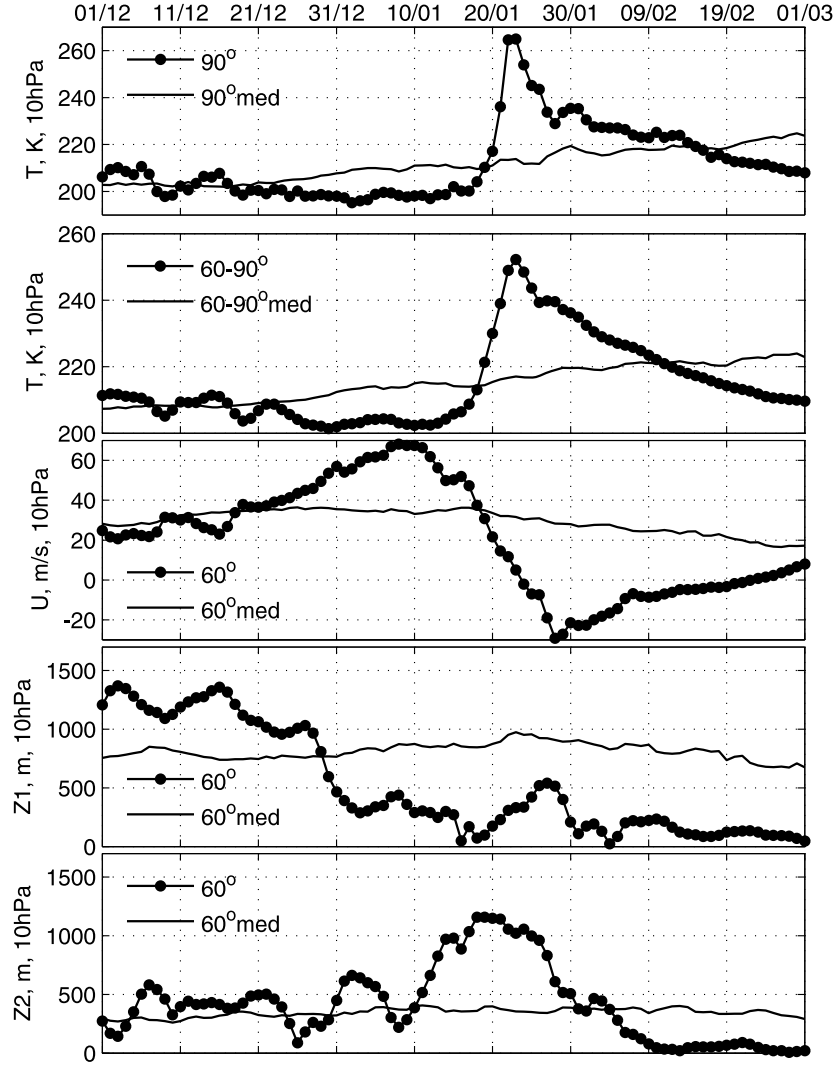


Figure 8: Stratospheric conditions for the winter of 2008–2009. Temperature at 90° N and 10 hPa (~ 32 km), zonal mean temperature at 60°–90°N , zonal mean zonal wind at 60°N, planetary wave 1 and 2 activity at 60°N and 10 hPa. Solid lines indicate 30-year means and solid circles indicate data for the winter of 2008–2009 (Figure 1, [Goncharenko et al., 2010](#)).

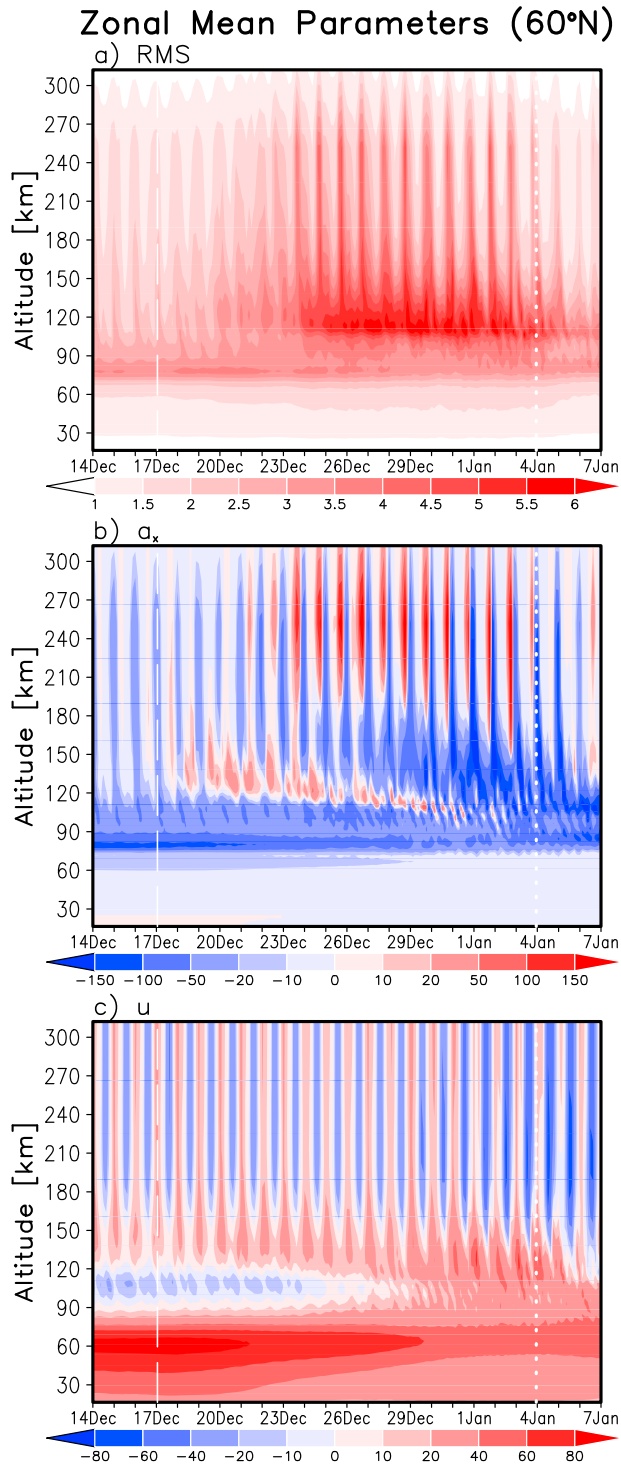


Figure 9: GCM simulation of the altitude-universal time variations of the zonal mean a) root-mean-square zonal wind (RMS, GW activity) in m s^{-1} , b) GW drag in $\text{m s}^{-1} \text{ day}^{-1}$, and c) large-scale zonal wind m s^{-1} , during a minor warming (Figure 2, [Yiğit and Medvedev, 2012](#)).

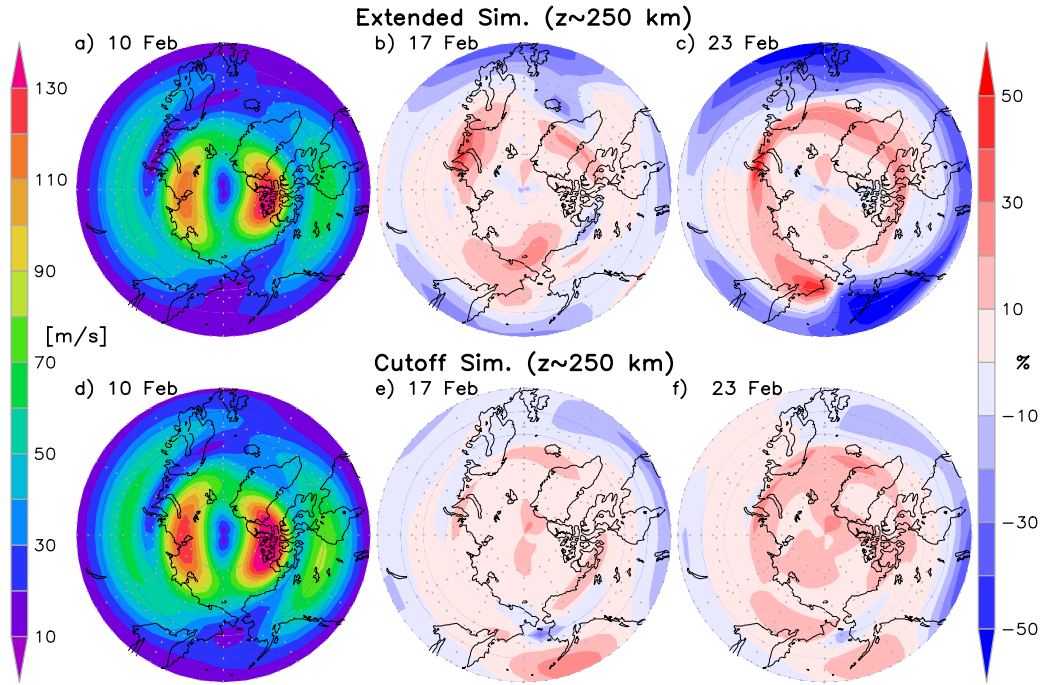


Figure 10: Northern Hemisphere polar stereographic projections at 250 km of small-scale variability on 10 Feb and the percentage changes (second and third columns from left) during the later phases of the warming in the extended (upper row) and the cut-off simulations (lower panels) (Figure 4, [Yiğit et al., 2014](#)).